Chapter 4

Finite Element Approximation

4.1 Introduction

Our goal in this chapter is the development of piecewise-polynomial approximations U of a two- or three-dimensional function u. For this purpose, it suffices to regard u as being known and to determine U as its interpolant on a domain Ω. Concentrating on two dimensions for the moment, let us partition Ω into a collection of finite elements and write U in the customary form

$$U(x,y) = \sum_{j=1}^{N} c_j \phi_j(x,y). \tag{4.1.1}$$

As we discussed, it is convenient to associate each basis function ϕ_j with a mesh entity, *e.g.*, a vertex, edge, or element in two dimensions and a vertex, edge, face, or element in three dimensions. We will discuss these entities and their hierarchical relationship further in Chapter 5. For now, if ϕ_j is associated with the entity indexed by j, then, as described in Chapters 1 and 2, finite element bases are constructed so that ϕ_j is nonzero only on elements containing entity j. The support of two-dimensional basis functions associated with a vertex, an edge, and an element interior is shown in Figure 4.1.1.

As in one dimension, finite element bases are constructed implicitly in an element-by-element manner in terms of "shape functions" (*cf.* Section 2.4). Once again, a shape function on an element e is the restriction of a basis function $\phi_j(x,y)$ to element e. We proceed by constructing shape functions on triangular elements (Section 4.2, 4.4), quadrilaterals (Sections 4.3, 4.4), tetrahedra (Section 4.5.1), and hexahedra (Section 4.5.2).

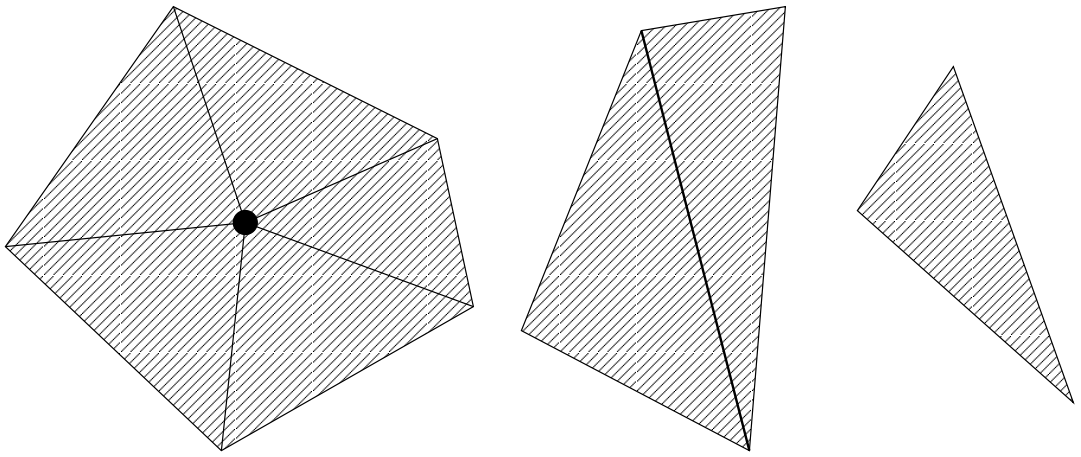

Figure 4.1.1: Support of basis functions associated with a vertex, edge, and element interior (left to right).

4.2 Lagrange Shape Functions on Triangles

Perhaps the simplest two-dimensional Lagrangian finite element basis is a piecewise-linear polynomial on a grid of triangular elements. It is the two-dimensional analog of the hat functions introduced in Section 1.3. Consider an arbitrary triangle e with its vertices indexed as 1, 2, and 3 and vertex j having coordinates (x_j, y_j), $j = 1, 2, 3$ (Figure 4.2.1). The linear shape function $N_j(x, y)$ associated with vertex j satisfies

$$N_j(x_k, y_k) = \delta_{j,k}, \qquad j, k = 1, 2, 3. \tag{4.2.1}$$

(Again, we omit the subscript e from $N_{j,e}$ whenever it is clear that we are discussing a single element.) Let N_j have the form

$$N_j(x, y) = a + bx + cy, \qquad (x, y) \in \Omega_e,$$

where Ω_e is the domain occupied by element e. Imposing conditions (4.2.1) produces

$$\begin{bmatrix} 1 \\ 0 \\ 0 \end{bmatrix} = \begin{bmatrix} 1 & x_j & y_j \\ 1 & x_k & y_k \\ 1 & x_l & y_l \end{bmatrix} \begin{bmatrix} a \\ b \\ c \end{bmatrix}, \qquad k \neq l \neq j, \qquad j, k, l = 1, 2, 3.$$

Solving this system by Crammer's rule yields

$$N_j(x, y) = \frac{D_{k,l}(x, y)}{C_{j,k,l}}, \qquad k \neq l \neq j, \qquad j, k, l = 1, 2, 3, \tag{4.2.2a}$$

where

$$D_{k,l} = \det \begin{bmatrix} 1 & x & y \\ 1 & x_k & y_k \\ 1 & x_l & y_l \end{bmatrix}, \tag{4.2.2b}$$

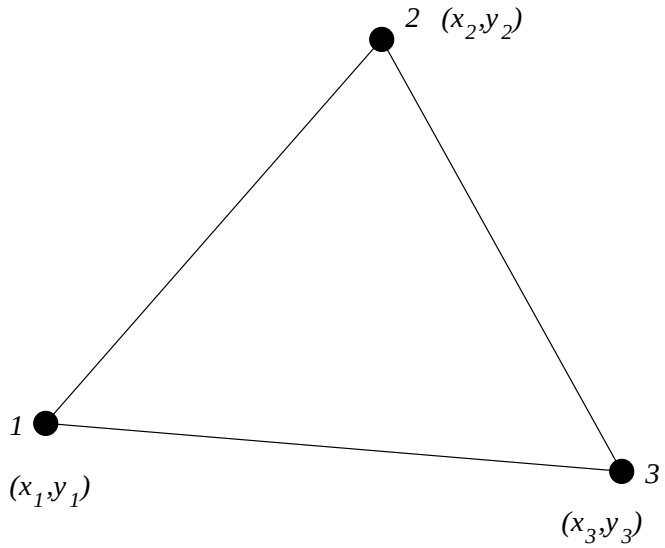

Figure 4.2.1: Triangular element with vertices $1, 2, 3$ having coordinates (x_1, y_1), (x_2, y_2), and (x_3, y_3).

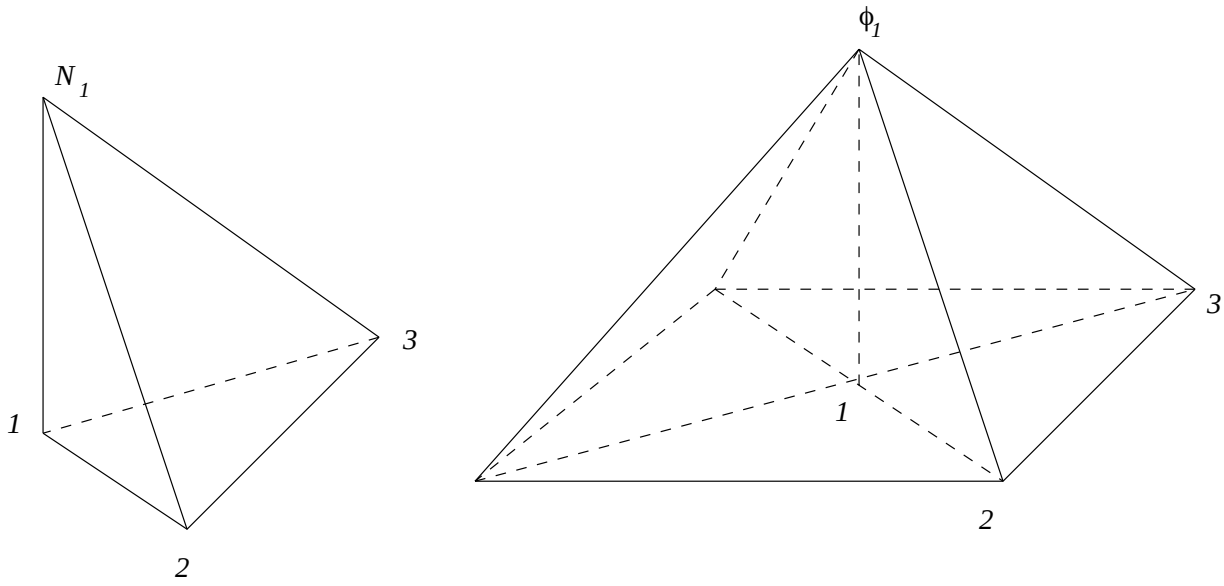

Figure 4.2.2: Shape function N_1 for Node 1 of element e (left) and basis function ϕ_1 for a cluster of four finite elements at Node 1.

$$C_{j,k,l} = \det \begin{bmatrix} 1 & x_j & y_j \\ 1 & x_k & y_k \\ 1 & x_l & y_l \end{bmatrix} . \tag{4.2.2c}$$

Basis functions are constructed by combining shape functions on neighboring elements as described in Section 2.4. A sample basis function for a four-element cluster is shown in Figure 4.2.2. The implicit construction of the basis in terms of shape function eliminates the need to know detailed geometric information such as the number of elements sharing

a node. Placing the three nodes at element vertices guarantees a continuous basis. While interpolation at three non-colinear points is (necessary and) sufficient to determine a unique linear polynomial, it will not determine a continuous approximation. With vertex placement, the shape function (*e.g.*, N_j) along any element edge is a linear function of a variable along that edge. This linear function is determined by the nodal values at the two vertex nodes on that edge (*e.g.*, j and k). As shown in Figure 4.2.2, the shape function on a neighboring edge is determined by the same two nodal values; thus, the basis (*e.g.*, ϕ_j) is continuous.

The restriction of $U(x, y)$ to element e has the form

$$U(x, y) = c_1 N_1(x, y) + c_2 N_2(x, y) + c_3 N_3(x, y), \qquad (x, y) \in \Omega_e. \tag{4.2.3}$$

Using (4.2.1), we have $c_j = U(x_j, y_j)$, $j = 1, 2, 3$.

The construction of higher-order Lagrangian shape functions proceeds in the same manner. In order to construct a $p\,th$-degree polynomial approximation on element e, we introduce $N_j(x, y)$, $j = 1, 2, \ldots, n_p$, shape functions at n_p nodes, where

$$n_p = \frac{(p + 1)(p + 2)}{2} \tag{4.2.4}$$

is the number of monomial terms in a complete polynomial of degree p in two dimensions. We may write a shape function in the form

$$N_j(x, y) = \sum_{i=1}^{n_p} a_i q_i(x, y) = \mathbf{a}^T \mathbf{q}(x, y) \tag{4.2.5a}$$

where

$$\mathbf{q}^T(x, y) = [1, x, y, x^2, xy, y^2, \ldots, y^p]. \tag{4.2.5b}$$

Thus, for example, a second degree ($p = 2$) polynomial would have $n_2 = 6$ coefficients and

$$\mathbf{q}^T(x, y) = [1, x, y, x^2, xy, y^2].$$

Including all n_p monomial terms in the polynomial approximation ensures isotropy in the sense that the degree of the trial function is conserved under coordinate translation and rotation.

With six parameters, we consider constructing a quadratic Lagrange polynomial by placing nodes at the vertices and midsides of a triangular element. The introduction of nodes is unnecessary, but it is a convenience. Indexing of nodes and other entities will be discussed in Chapter 5. Here, since we're dealing with a single element, we number the

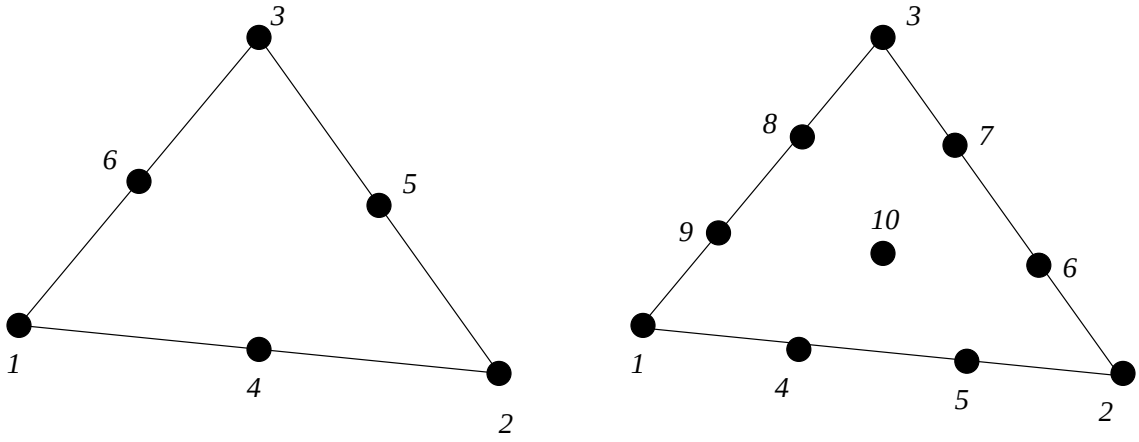

Figure 4.2.3: Arrangement of nodes for quadratic (left) and cubic (right) Lagrange finite element approximations.

nodes from 1 to 6 as shown in Figure 4.2.3. The shape functions have the form (4.2.5) with $n_2 = 6$

$$N_j = a_1 + a_2 x + a_3 y + a_4 x^2 + a_5 xy + a_6 y^2,$$

and the six coefficients a_j, $j = 1, 2, \ldots, 6$, are determined by requiring

$$N_j(x_k, y_k) = \delta_{j,k}, \qquad j, k = 1, 2, \ldots, 6.$$

The basis

$$\phi_j = \cup_{e=1}^{N_\Delta} N_{j,e}(x, y)$$

is continuous by virtue of the placement of the nodes. The shape function $N_{j,e}$ is a quadratic function of a local coordinate on each edge of the triangle. This quadratic function of a single variable is uniquely determined by the values of the shape functions at the three nodes on the given edge. Shape functions on shared edges of neighboring triangles are determined by the same nodal values; hence, ensuring that the basis is globally of class C^0.

The construction of cubic approximations would proceed in the same manner. A complete cubic in two dimensions has 10 parameters. These parameters can be determined by selecting 10 nodes on each element. Following the reasoning described above, we should place four nodes on each edge since a cubic function of one variable is uniquely determined by prescribing four quantities. This accounts for nine of the ten nodes. The last node can be placed at the centroid as shown in Figure 4.2.3.

The construction of Lagrangian approximations is straight forward but algebraically complicated. Complexity can be significantly reduced by using one of the following two coordinate transformations.

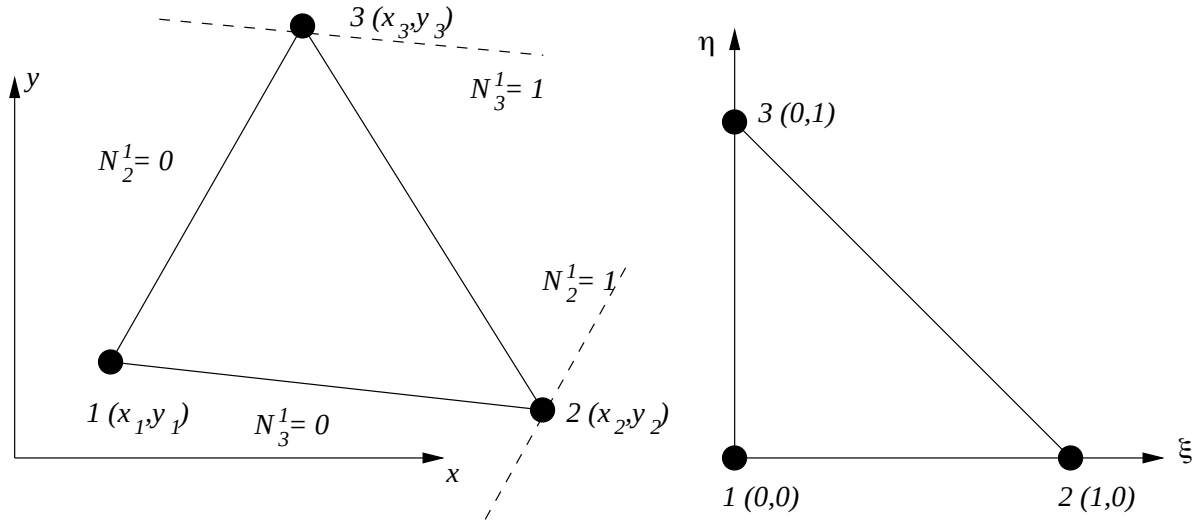

Figure 4.2.4: Mapping an arbitrary triangular element in the (x, y)-plane (left) to a canonical 45° right triangle in the (ξ, η)-plane (right).

1. Transformation to a canonical element. The idea is to transform an arbitrary element in the physical (x, y)-plane to one having a simpler geometry in a computational (ξ, η)-plane. For purposes of illustration, consider an arbitrary triangle having vertex nodes numbered 1, 2, and 3 which is mapped by a linear transformation to a unit 45° right triangle, as shown in Figure 4.2.4.

Consider N_2^1 and N_3^1 as defined by (4.2.2). (A superscript 1 has been added to emphasize that the shape functions are linear polynomials.) The equation of the line connecting Nodes 1 and 3 of the triangular element shown on the left of Figure 4.2.4 is $N_2^1 = 0$. Likewise, the equation of a line passing through Node 2 and parallel to the line passing through Nodes 1 and 3 is $N_2^1 = 1$. Thus, to map the line $N_2^1 = 0$ onto the line $\xi = 0$ in the canonical plane, we should set $\xi = N_2^1(x, y)$. Similarly, the line joining Nodes 1 and 2 satisfies the equation $N_3^1 = 0$. We would like this line to become the line $\eta = 0$ in the transformed plane, so our mapping must be $\eta = N_3^1(x, y)$. Therefore, using (4.2.2)

$$\xi = N_2^1(x,y) = \frac{\det\begin{bmatrix} 1 & x & y \\ 1 & x_1 & y_1 \\ 1 & x_3 & y_3 \end{bmatrix}}{\det\begin{bmatrix} 1 & x_2 & y_2 \\ 1 & x_1 & y_1 \\ 1 & x_3 & y_3 \end{bmatrix}}, \qquad \eta = N_3^1(x,y) = \frac{\det\begin{bmatrix} 1 & x & y \\ 1 & x_1 & y_1 \\ 1 & x_2 & y_2 \end{bmatrix}}{\det\begin{bmatrix} 1 & x_3 & y_3 \\ 1 & x_1 & y_1 \\ 1 & x_2 & y_2 \end{bmatrix}}. \tag{4.2.6}$$

As a check, evaluate the determinants and verify that $(x_1, y_1) \to (0, 0)$, $(x_2, y_2) \to (1, 0)$, and $(x_3, y_3) \to (0, 1)$.

Polynomials may now be developed on the canonical triangle to simplify the algebraic

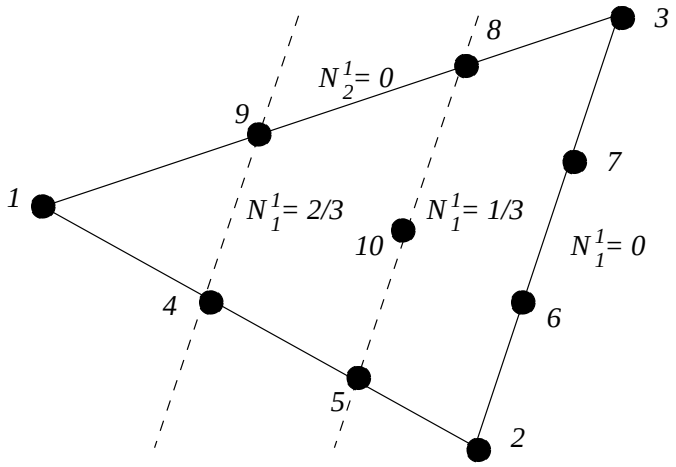

Figure 4.2.5: Geometry of a triangular finite element for a cubic polynomial Lagrange approximation.

complexity and subsequently transformed back to the physical element.

2. Transformation using triangular coordinates. A simple procedure for constructing Lagrangian approximations involves the use of a redundant coordinate system. The construction may be described in general terms, but an example suffices to illustrate the procedure. Thus, consider the construction of a cubic approximation on the triangular element shown in Figure 4.2.5. The vertex nodes are numbered 1, 2, and 3; edge nodes are numbered 4 to 9; and the centroid is numbered as Node 10.

Observe that

- the line $N_1^1 = 0$ passes through Nodes 2, 6, 7, and 3;
- the line $N_1^1 = 1/3$ passes through Nodes 5, 10, and 8; and
- the line $N_1^1 = 2/3$ passes through Nodes 4 and 9.

Since N_1^3 must vanish at Nodes 2 - 10 and be a cubic polynomial, it must have the form

$$N_1^3(x, y) = \alpha N_1^1(N_1^1 - 1/3)(N_1^1 - 2/3)$$

where the constant α is determined by normalizing $N_1^3(x_1, y_1) = 1$. Since $N_1^1(x_1, y_1) = 1$, we find $\alpha = 9/2$ and

$$N_1^3(x, y) = \frac{9}{2} N_1^1(N_1^1 - 1/3)(N_1^1 - 2/3).$$

The shape function for an edge node is constructed in a similar manner. For example, in order to obtain N_4^3 we observe that

- the line $N_2^1 = 0$ passes through Nodes 1, 9, 8, and 3;

- the line $N_1^1 = 0$ passes through Nodes 2, 6, 7, and 3; and
- the line $N_1^1 = 1/3$ passes through Nodes 5, 10, and 8.

Thus, N_4^3 must have the form

$$N_4^3(x,y) = \alpha N_1^1 N_2^1 (N_1^1 - 1/3).$$

Normalizing $N_4^3(x_4, y_4) = 1$ gives

$$N_4^3(x_4,y_4) = \alpha \frac{2}{3}\frac{1}{3}(\frac{2}{3} - \frac{1}{3}).$$

Hence, $\alpha = 27/2$ and

$$N_4^3(x,y) = \frac{27}{2} N_1^1 N_2^1 (N_1^1 - 1/3).$$

Finally, the shape function N_{10}^3 must vanish on the boundary of the triangle and is, thus, determined as

$$N_{10}^3(x,y) = 27 N_1^1 N_2^1 N_3^1.$$

The cubic shape functions N_1^3, N_4^3, and N_{10}^3 are shown in Figure 4.2.6.

The three linear shape functions N_j^1, $j = 1, 2, 3$, can be regarded as a redundant coordinate system known as "triangular" or "barycentric" coordinates. To be more specific, consider an arbitrary triangle with vertices numbered 1, 2, and 3 as shown in Figure 4.2.7. Let

$$\zeta_1 = N_1^1, \qquad \zeta_2 = N_2^1, \qquad \zeta_3 = N_3^1, \tag{4.2.7}$$

and define the transformation from triangular to physical coordinates as

$$\begin{bmatrix} x \\ y \\ 1 \end{bmatrix} = \begin{bmatrix} x_1 & x_2 & x_3 \\ y_1 & y_2 & y_3 \\ 1 & 1 & 1 \end{bmatrix} \begin{bmatrix} \zeta_1 \\ \zeta_2 \\ \zeta_3 \end{bmatrix}. \tag{4.2.8}$$

Observe that $(\zeta_1, \zeta_2, \zeta_3)$ has value (1,0,0) at vertex 1, (0,1,0) at vertex 2 and (0,0,1) at vertex 3.

An alternate, and more common, definition of the triangular coordinate system involves ratios of areas of subtriangles to the whole triangle. Thus, let P be an arbitrary point in the interior of the triangle, then the triangular coordinates of P are

$$\zeta_1 = \frac{A_{P23}}{A_{123}}, \qquad \zeta_2 = \frac{A_{P31}}{A_{123}}, \qquad \zeta_3 = \frac{A_{P12}}{A_{123}}, \tag{4.2.9}$$

where A_{123} is the area of the triangle, A_{P23} is the area of the subtriangle having vertices P, 2, 3, *etc.*

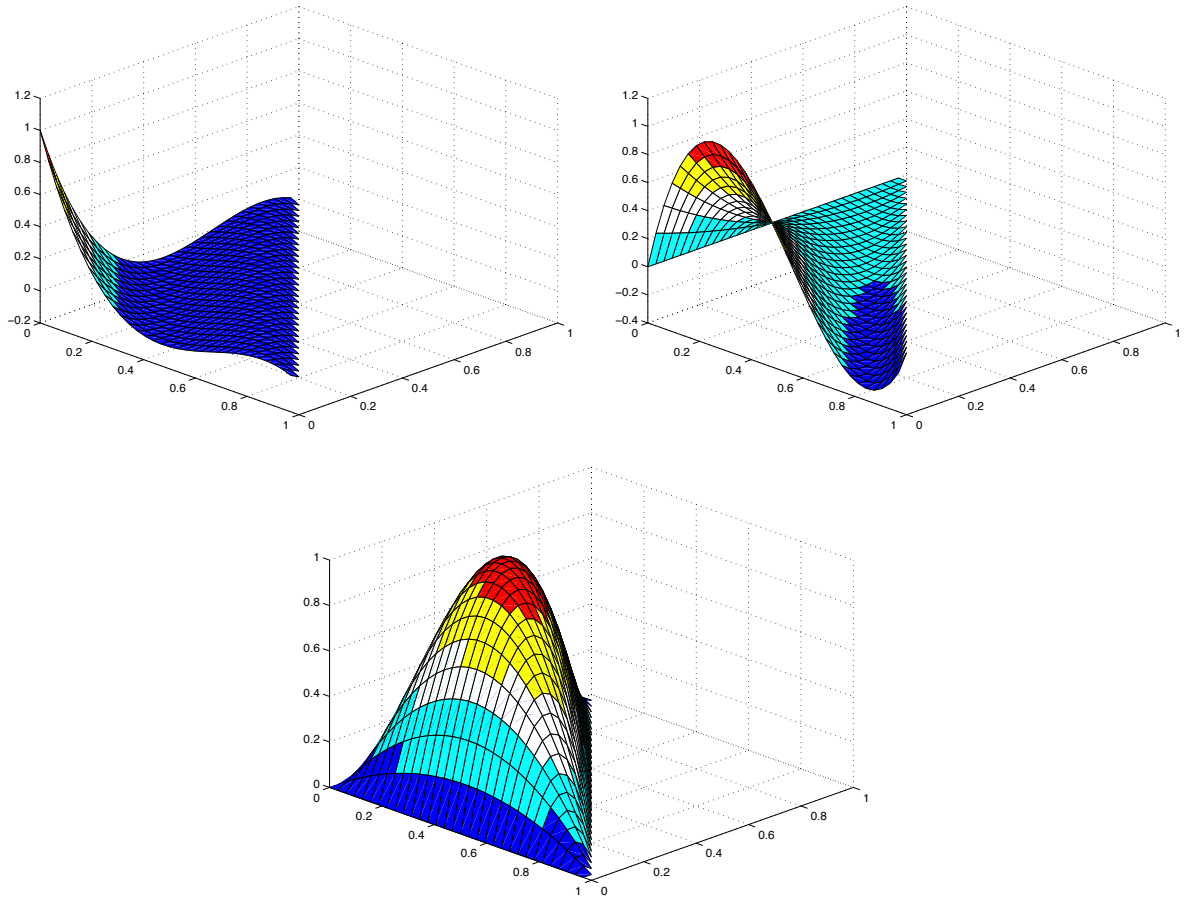

Figure 4.2.6: Cubic Lagrange shape functions associated with a vertex (left), an edge(right), and the centroid (bottom) of a right 45° triangular element.

The triangular coordinate system is redundant since two quantities suffice to locate a point in a plane. This redundancy is expressed by the third of equations (4.2.8), which states that

$$\zeta_1 + \zeta_2 + \zeta_3 = 1.$$

This relation also follows by adding equations (4.2.9).

Although seemingly distinct, triangular coordinates and the canonical coordinates are closely related. The triangular coordinate ζ_2 is equivalent to the canonical coordinate ξ and ζ_3 is equivalent to η, as seen from (4.2.6) and (4.2.7).

Problems

1. With reference to the nodal placement and numbering shown on the left of Figure 4.2.3, construct the shape functions for Nodes 1 and 4 of the quadratic Lagrange polynomial. Derive your answer using triangular coordinates. Having done this, also express your answer in terms of the canonical (ξ, η) coordinates. Plot or sketch

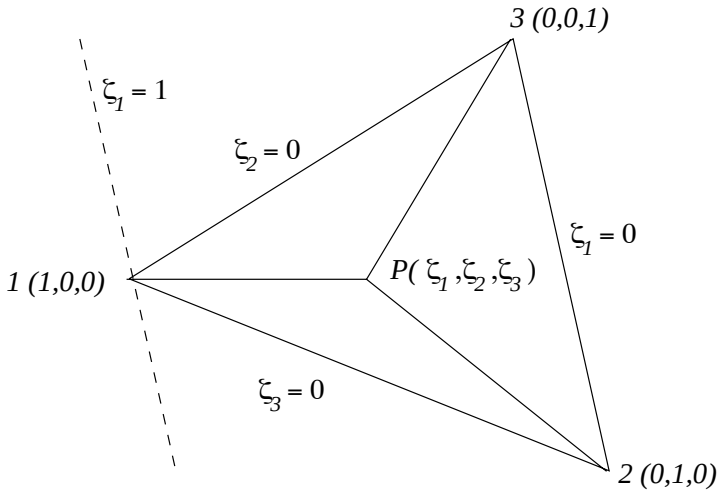

Figure 4.2.7: Triangular coordinate system.

the two shape functions on the canonical element.

2. A Lagrangian approximation of degree p on a triangle has three nodes at the vertices and $p-1$ nodes along each edge that are not at vertices. As we've discussed, the latter placement ensures continuity on a mesh of triangular elements. If no additional nodes are placed on edges, how many nodes are interior to the element if the approximation is to be complete?

4.3 Lagrange Shape Functions on Rectangles

The triangle in two dimensions and the tetrahedron in three dimensions are the polyhedral shapes having the minimum number of edges and faces. They are optimal for defining complete C^0 Lagrangian polynomials. Even so, Lagrangian interpolants are simple to construct on rectangles and hexahedra by taking products of one-dimensional Lagrange polynomials. Multi-dimensional polynomials formed in this manner are called "tensor-product" approximations. we'll proceed by constructing polynomial shape functions on canonical 2×2 square elements and mapping these elements to an arbitrary quadrilateral elements. We describe a simple bilinear mapping here and postpone more complex mappings to Chapter 5.

We consider the canonical 2×2 square $\{(\xi, \eta) | -1 \leq \xi, \eta \leq 1\}$ shown in Figure 4.3.1. For simplicity, the vertices of the element have been indexed with a double subscript as $(1,1)$, $(2,1)$, $(1,2)$, and $(2,2)$. At times it will be convenient to index the vertex coordinats as $\xi_1 = -1$, $\xi_2 = 1$, $\eta_1 = -1$, and $\eta_2 = 1$. With nodes at each vertex, we construct a bilinear Lagrangian polynomial $U(\xi, \eta)$ whose restriction to the canonical

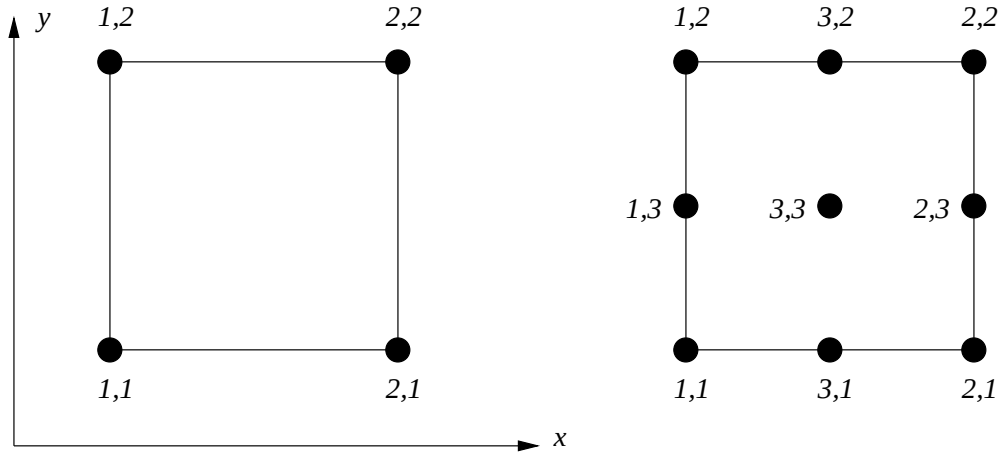

Figure 4.3.1: Node indexing for canonical square elements with bilinear (left) and biquadratic (right) polynomial shape functions.

element has the form

$$U(\xi,\eta) = c_{1,1}N_{1,1}(\xi,\eta) + c_{2,1}N_{2,1}(\xi,\eta) + c_{2,2}N_{2,2}(\xi,\eta) + c_{1,2}N_{1,2}(\xi,\eta). \tag{4.3.1a}$$

As with Lagrangian polynomials on triangles, the shape function $N_{i,j}(\xi,\eta)$ satisfies

$$N_{i,j}(\xi_k,\eta_l) = \delta_{i,k}\delta_{j,l}, \qquad k,l = 1,2. \tag{4.3.1b}$$

Once again, $U(\xi_k,\eta_l) = c_{k,l}$; however, now $N_{i,j}$ is the product of one-dimensional hat functions

$$N_{i,j}(\xi,\eta) = \bar{N}_i(\xi)\bar{N}_j(\eta) \tag{4.3.1c}$$

with

$$\bar{N}_1(\xi) = \frac{1-\xi}{2}, \tag{4.3.1d}$$

$$\bar{N}_2(\xi) = \frac{1+\xi}{2}, \qquad -1 \le \xi \le 1. \tag{4.3.1e}$$

Similar formulas apply to $\bar{N}_j(\eta)$, $j = 1,2$, with ξ replaced by η and i replaced by j. The shape function $N_{1,1}$ is shown in Figure 4.3.2. By examination of either this figure or (4.3.1c-e), we see that $N_{i,j}(\xi,\eta)$ is a bilinear function of the form

$$N_{i,j}(\xi,\eta) = a_1 + a_2\xi + a_3\eta + a_4\xi\eta, \qquad -1 \le \xi,\eta \le 1. \tag{4.3.2}$$

The shape function is linear along the two edges containing node (i,j) and it vanishes along the two opposite edges.

A basis may be constructed by uniting shape functions on elements sharing a node. The piecewise bilinear basis functions $\phi_{i,j}$ when Node (i,j) is at the intersection of four

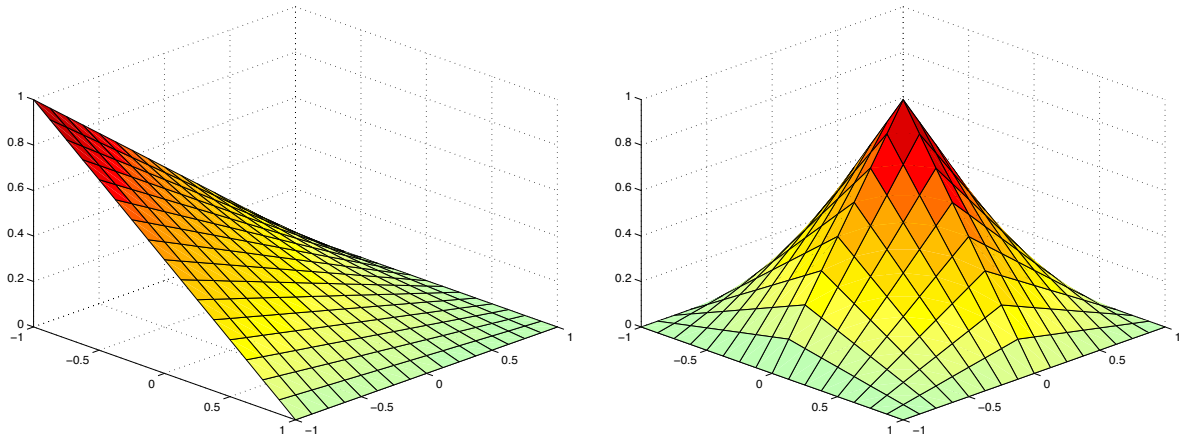

Figure 4.3.2: Bilinear shape function $N_{1,1}$ on the $[-1,1]\times[-1,1]$ canonical square element (left) and bilinear basis function at the intersection of four square elements (right).

square elements is shown in Figure 4.3.2. Since each shape function is a linear polynomial along element edges, the basis will be continuous on a grid of square (or rectangular) elements. The restriction to a square (or rectangular) grid is critical and the approximation would *not* be continuous on an arbitrary mesh of quadrilateral elements.

To construct biquadratic shape functions on the canonical square, we introduce 9 nodes: (1,1), (2,1), (2,2), and (1,2) at the vertices; (3,1), (2,3), (3,2), and (1,3) at midsides; and (3,3) at the center (Figure 4.3.1). The restriction of the interpolant U to this element has the form

$$U(\xi,\eta) = \sum_{i=1}^{3}\sum_{j=1}^{3} c_{i,j} N_{i,j}(\xi,\eta) \tag{4.3.3a}$$

where the shape functions $N_{i,j}$, $i,j = 1,2,3$, are products of the one-dimensional quadratic polynomial Lagrange shape functions

$$N_{i,j}(\xi,\eta) = \bar{N}_i(\xi)\bar{N}_j(\eta), \qquad i,j = 1,2,3, \tag{4.3.3b}$$

with (*cf.* Section 2.4)

$$\bar{N}_1(\xi) = -\xi(1-\xi)/2, \tag{4.3.3c}$$

$$\bar{N}_2(\xi) = \xi(1+\xi)/2, \tag{4.3.3d}$$

$$\bar{N}_3(\xi) = (1-\xi^2), \qquad -1 \le \xi \le 1. \tag{4.3.3e}$$

Shape functions for a vertex, an edge, and the centroid are shown in Figure 4.3.3. Using (4.3.3b-e), we see that shape functions are biquadratic polynomials of the form

$$N_{i,j}(\xi,\eta) = a_1 + a_2\xi + a_3\eta + a_4\xi^2 + a_5\xi\eta + a_6\eta^2 + a_7\xi\eta^2 + a_8\xi^2\eta + a_9\xi^2\eta^2. \tag{4.3.4}$$

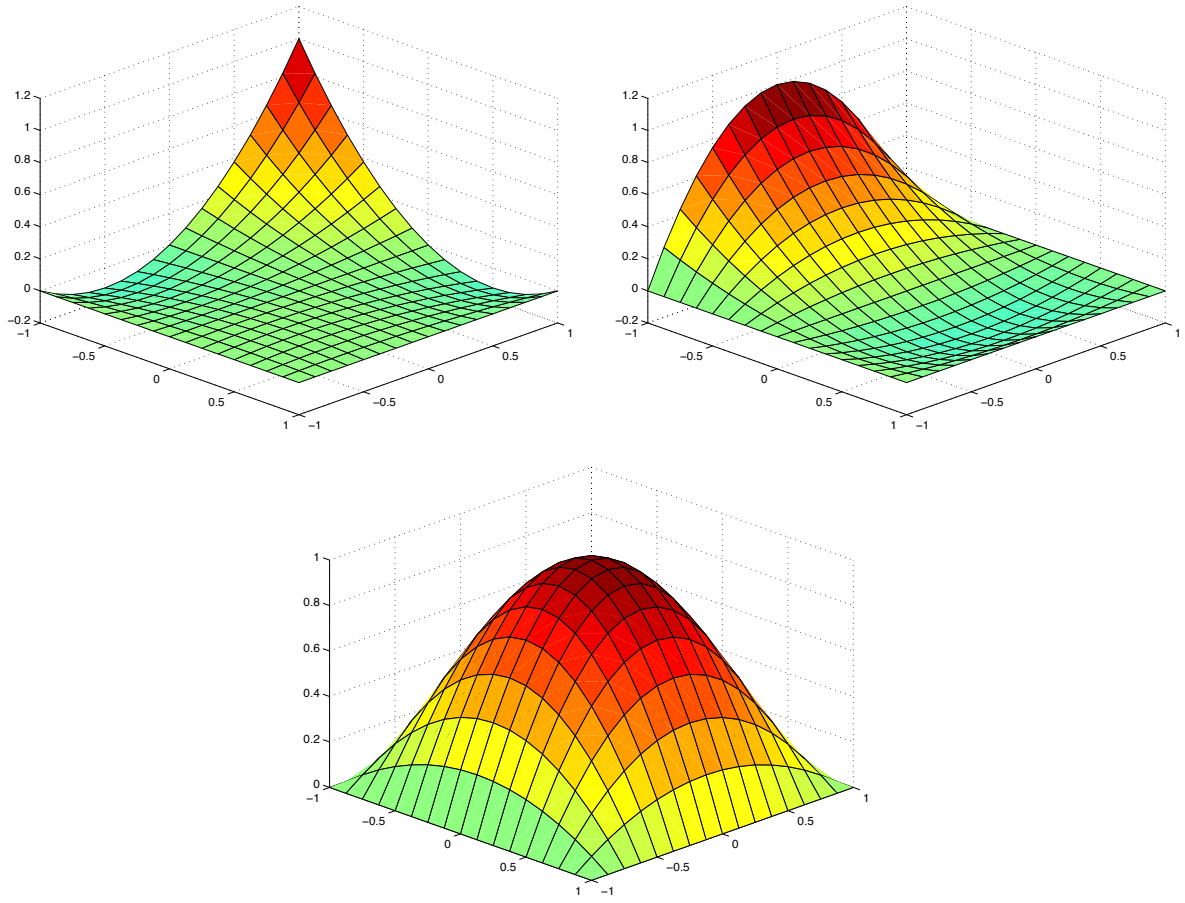

Figure 4.3.3: Biquadratic shape functions associated with a vertex (left), an edge (right), and the centroid (bottom).

Although (4.3.4) contains some cubic and quartic monomial terms, interpolation accuracy is determined by the highest-degree *complete* polynomial that can be represented exactly, which, in this case, is a quadratic polynomial.

Higher-order shape functions are constructed in similar fashion.

4.3.1 Bilinear Coordinate Transformations

Shape functions on the canonical square elements may be mapped to arbitrary quadrilaterals by a variety of transformations (*cf.* Chapter 5). The simplest of these is a picewise-bilinear function that uses the same shape functions (4.3.1d,e) as the finite element solution (4.3.1a). Thus, consider a mapping of the canonical 2×2 square S to a quadrilateral Q having vertices at $(x_{i,j}, y_{i,j})$, $i, j = 1, 2$, in the physical (x, y)-plane (Figure 4.3.4) using a bilinear transformation written in terms of (4.3.1d,e) as

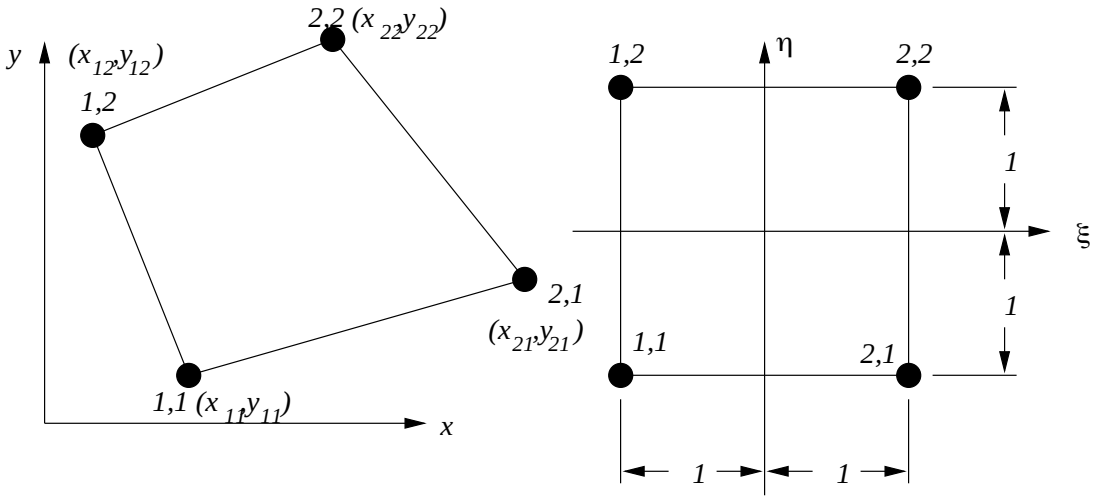

Figure 4.3.4: Bilinear mapping of the canonical square to a quadrilateral.

$$\begin{bmatrix} x(\xi,\eta) \\ y(\xi,\eta) \end{bmatrix} = \sum_{i=1}^{2}\sum_{j=1}^{2} \begin{bmatrix} x_{ij} \\ y_{ij} \end{bmatrix} N_{i,j}(\xi,\eta), \tag{4.3.5}$$

where $N_{i,j}(\xi,\eta)$ is given by (4.3.1b).

The transformation is linear on each edge of the element. In particular, transforming the edge $\eta = -1$ to the physical edge $(x_{11}, y_{11}$ - $(x_{21}, y21)$ yields

$$\begin{bmatrix} x \\ y \end{bmatrix} = \begin{bmatrix} x_{11} \\ y_{11} \end{bmatrix} \frac{1-\xi}{2} + \begin{bmatrix} x_{21} \\ y_{21} \end{bmatrix} \frac{1+\xi}{2}, \qquad -1 \le \xi \le 1.$$

As ξ varies from -1 to 1, x and y vary linearly from (x_{11}, y_{11}) to (x_{21}, y_{21}). The locations of the vertices (1,2) and (2,2) have no effect on the transformation. This ensures that a continuous approximation in the (ξ,η)-plane will remain continuous when mapped to the (x,y)-plane. We have to ensure that the mapping is invertible and we'll show in Chapter 5 that this is the case when Q is convex.

Problems

1. As noted, interpolation errors of the biquadratic approximation (4.3.3) are the same order as for a quadratic approximation on a triangle. Thus, for example, the L^2 error in interpolating a smooth function $u(x,y)$ by a piecewise biquadratic function $U(x,y)$ is $O(h^3)$, where h is the length of the longest edge of an element. The extra degrees of freedom associated with the cubic and quartic terms do not generally improve the order of accuracy. Hence, we might try to eliminate some shape functions and reduce the complexity of the approximation. Unknowns associated with interior shape functions are only coupled to unknowns on the element and can easily be eliminated by a variety of techniques. Considering the biquadratic polynomial in the form (4.3.3a), we might determine $c_{3,3}$ so that the coefficient of the

quartic term x^2y^2 vanishes. Show how this may be done for a 2×2 square canonical element. Polynomials of this type have been called *serendipity* by Zienkiewicz [8]. In the next section, we shall see that they are also a part of the hierarchical family of approximations. The parameter $c_{3,3}$ is said to be "constrained" since it is prescribed in advance and not determined as part of the Galerkin procedure. Plot or sketch shape functions associated with a vertex and a midside.

4.4 Hierarchical Shape Functions

We have discussed the advantages of hierarchical bases relative to Lagrangian bases for one-dimensional problems in Section 2.5. Similar advantages apply in two and three dimensions. We'll again use the basis of Szabó and Babuška [7], but follow the construction procedure of Shephard *et al.* [6] and Dey *et al.* [5]. Hierarchical bases of degree p may be constructed for triangles and squares. Squares are the simpler of the two, so let us handle them first.

4.4.1 Hierarchical Shape Functions on Squares

We'll construct the basis on the canonical element $\{(\xi,\eta)| -1 \le \xi,\eta \le 1\}$, indexing the vertices, edges, and interiors as described for the biquadratic approximation shown in Figure 4.3.1. The hierarchical polynomial of order p has a basis consisting of the following shape functions.

Vertex shape functions. The four vertex shape functions are the bilinear functions (4.3.1c-e)

$$N^1_{i,j} = \bar{N}_i(\xi)\bar{N}_j(\eta), \qquad i,j = 1,2, \tag{4.4.1a}$$

where

$$\bar{N}_1(\xi) = \frac{1-\xi}{2}, \qquad \bar{N}_2(\xi) = \frac{1+\xi}{2}. \tag{4.4.1b}$$

The shape function $N^1_{1,1}$ is shown in the upper left portion of Figure 4.4.1.

Edge shape functions. For $p \ge 2$, there are $4(p-1)$ shape functions associated with the midside nodes $(3,1)$, $(2,3)$, $(3,2)$, and $(1,3)$:

$$N^k_{3,1}(\xi,\eta) = \bar{N}_1(\eta)\bar{N}^k(\xi), \tag{4.4.2a}$$
$$N^k_{3,2}(\xi,\eta) = \bar{N}_2(\eta)\bar{N}^k(\xi), \tag{4.4.2b}$$
$$N^k_{1,3}(\xi,\eta) = \bar{N}_1(\xi)\bar{N}^k(\eta), \tag{4.4.2c}$$
$$N^k_{2,3}(\xi,\eta) = \bar{N}_2(\xi)\bar{N}^k(\eta), \qquad k = 2,3,\ldots,p, \tag{4.4.2d}$$

where $\bar{N}^k(\xi)$, $k = 2, 3, \ldots, p$, are the one-dimensional hierarchical shape functions given by (2.5.8a) as

$$\bar{N}^k(\xi) = \sqrt{\frac{2k-1}{2}} \int_{-1}^{\xi} P_{k-1}(\sigma) d\sigma. \tag{4.4.2e}$$

Edge shape functions $N^k_{3,1}$ are shown for $k = 2, 3, 4$, in Figure 4.4.1. The edge shape functions are the product of a linear function of the variable normal to the edge to which they are associated and a hierarchical polynomial of degree k in a variable on this edge. The linear function ($\bar{N}_j(\xi)$, $\bar{N}_j(\eta)$, $j = 1, 2$) "blends" the edge function ($\bar{N}^k(\xi)$, $\bar{N}^k(\eta)$) onto the element so as to ensure continuity of the basis.

Interior shape functions. For $p \geq 4$, there are $(p-2)(p-3)/2$ internal shape functions associated with the centroid, Node $(3, 3)$. The first internal shape function is the "bubble function"

$$N^{4,0,0}_{3,3} = (1 - \xi^2)(1 - \eta^2). \tag{4.4.3a}$$

The remaining shape functions are products of $N^{4,0,0}_{3,3}$ and the Legendre polynomials as

$$\begin{aligned}
N^{5,1,0}_{3,3} &= N^{4,0,0}_{3,3} P_1(\xi), && (4.4.3b)\\
N^{5,0,1}_{3,3} &= N^{4,0,0}_{3,3} P_1(\eta), && (4.4.3c)\\
N^{6,2,0}_{3,3} &= N^{4,0,0}_{3,3} P_2(\xi), && (4.4.3d)\\
N^{6,1,1}_{3,3} &= N^{4,0,0}_{3,3} P_1(\xi) P_1(\eta), && (4.4.3e)\\
N^{6,0,2}_{3,3} &= N^{4,0,0}_{3,3} P_2(\eta), \qquad \ldots. && (4.4.3f)
\end{aligned}$$

The superscripts k, λ, and μ, resectively, give the polynomial degree, the degree of $P_\lambda(\xi)$, and the degree of $P_\mu(\eta)$. The first six interior bubble shape functions $N^{k,\lambda,\mu}_{3,3}$, $\lambda+\mu = k-4$, $k = 4, 5, 6$, are shown in Figure 4.4.2. These functions vanish on the element boundary to maintain continuity.

On the canonical element, the interpolant $U(\xi, \eta)$ is written as the usual linear combination of shape functions

$$U(\xi,\eta) = \sum_{i=1}^{2}\sum_{j=1}^{2} c^1_{i,j} N^1_{i,j} + \sum_{k=2}^{p}[\sum_{j=1}^{2} c^k_{3,j} N^k_{3,j} + \sum_{i=1}^{2} c^k_{i,3} N^k_{i,3}] + \sum_{k=4}^{p} \sum_{\lambda+\mu=k-4} c^{k,\lambda,\mu}_{3,3} N^{k,\lambda,\mu}_{3,3}. \tag{4.4.4}$$

The notation is somewhat cumbersome but it is explicit. The first summation identifies unknowns and shape functions associated with vertices. The two center summations identify edge unknowns and shape functions for polynomial orders 2 to p. And, the third summation identifies the interior unknowns and shape functions of orders 4 to p.

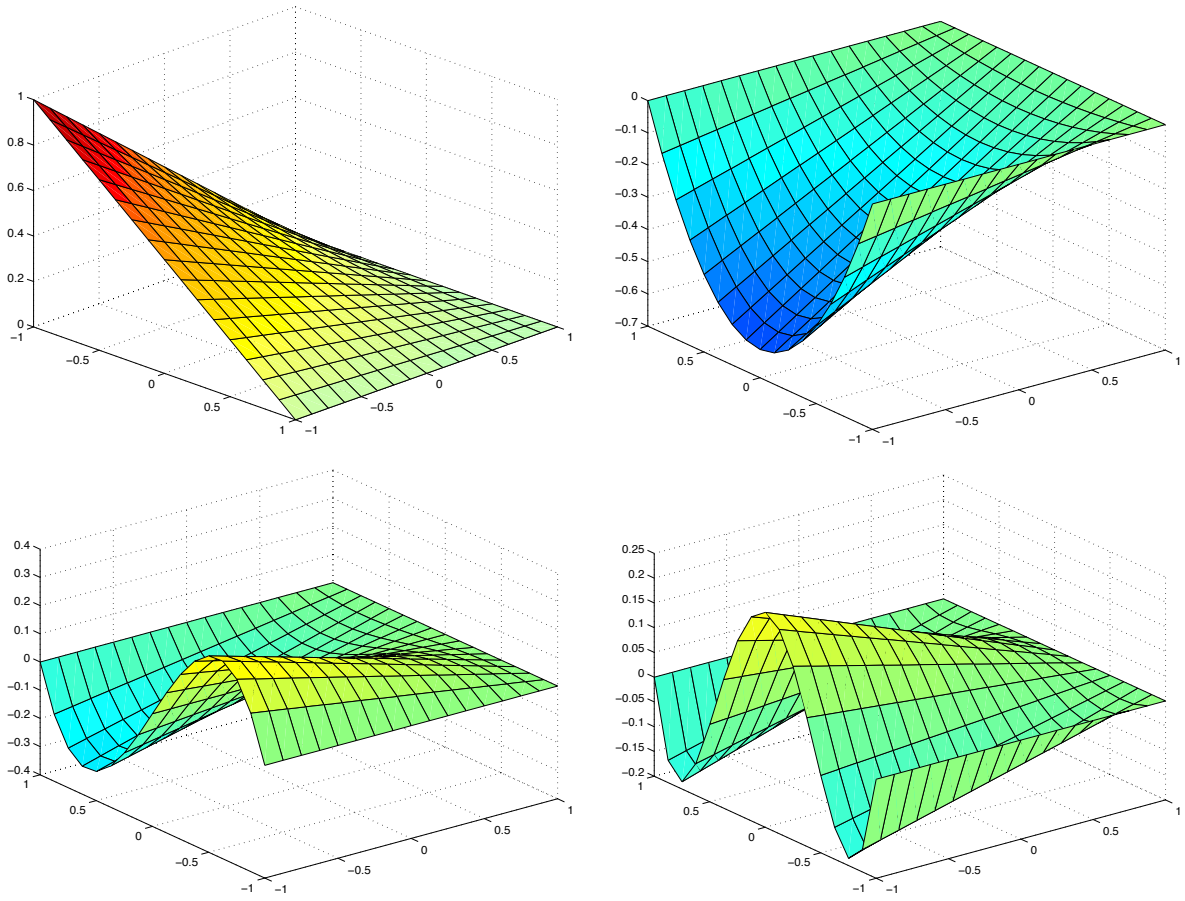

Figure 4.4.1: Hierarchical vertex and edge shape functions for $k = 1$ (upper left), $k = 2$ (upper right), $k = 3$ (lower left), and $k = 4$ (lower right).

Summations are understood to be zero when their initial index exceeds the final index. A degree p approximation has $4 + 4(p-1)_+ + (p-2)_+(p-3)_+/2$ unknowns and shape functions, where $q_+ = \max(q, 0)$. This function is listed in Table 4.4.1 for p ranging from 1 to 8. For large values of p there are $O(p^2)$ internal shape functions and $O(p)$ edge functions.

4.4.2 Hierarchical Shape Functions on Triangles

We'll express the hierarchical shape functions for triangular elements in terms of triangular coordinates, indexing the vertices as 1, 2, and 3; the edges as 4, 5, and 6; and the centroid as 7 (Figure 4.4.3). The basis consists of the following shape functions.

Vertex Shape functions. The three vertex shape functions are the linear barycentric coordinates (4.2.7)

$$N_i^1(\zeta_1, \zeta_2, \zeta_3) = \zeta_i, \qquad i = 1, 2, 3. \tag{4.4.5}$$

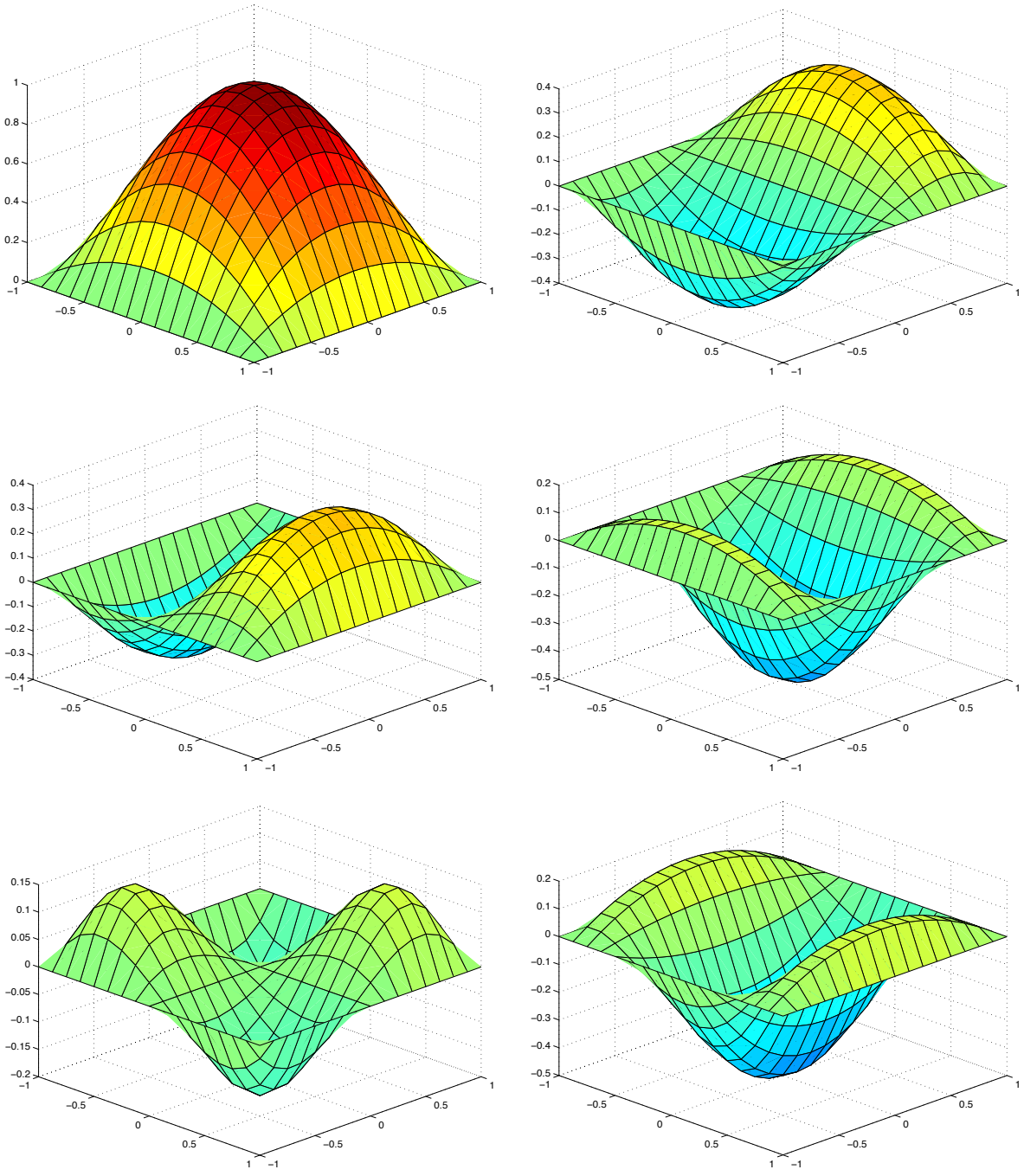

Figure 4.4.2: Hierarchical interior shape functions $N_{3,3}^{4,0,0}$, $N_{3,3}^{5,1,0}$ (top), $N_{3,3}^{5,0,1}$, $N_{3,3}^{6,2,0}$ (middle), and $N_{3,3}^{6,1,1}$, $N_{3,3}^{6,0,2}$ (bottom).

p	Square Dimension	Triangle Dimension
1	4	3
2	8	6
3	12	10
4	17	15
5	23	21
6	30	28
7	38	36
8	47	45

Table 4.4.1: Dimension of the hierarchical basis of order p on square and triangular elements.

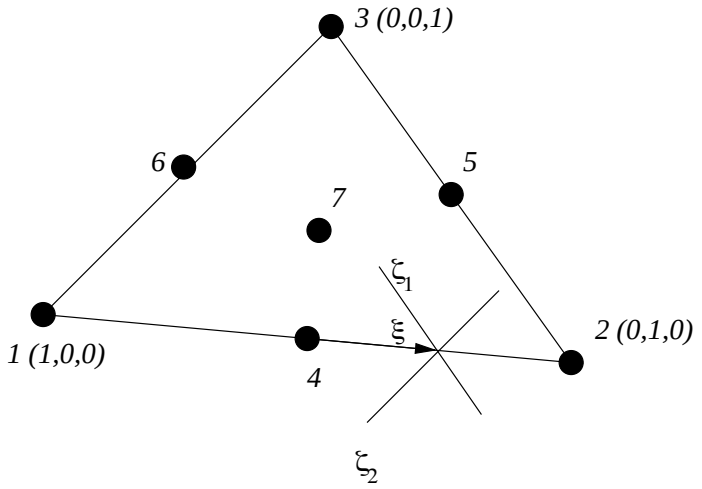

Figure 4.4.3: Node placement and coordinates for hierarchical approximations on a triangle.

Edge shape functions. For $p \geq 2$ there are $3(p-1)$ edge shape functions which are each nonzero on one edge (to which they are associated) and vanish on the other two. Each shape function is selected to match the corresponding edge shape function on a square element so that a continuous approximation may be obtained on meshes with both triangular and quadrilateral elements. Let us construct of the shape functions N_4^k, $k = 2, 3, \ldots, p$, associated with Edge 4. They are required to vanish on Edges 5 and 6 and must have the form

$$N_4^k(\zeta_1, \zeta_2, \zeta_3) = \zeta_1 \zeta_2 \bar{\chi}^k(\xi), \qquad k = 2, 3, \ldots, p, \tag{4.4.6a}$$

where $\bar{\chi}^k(\xi)$ is a shape function to be determined and ξ is a coordinate on Edge 4 that has value -1 at Node 1, 0 at Node 4, and 1 at Node 2. Since Edge 4 is $\zeta_3 = 0$, we have

$$N_4^k(\zeta_1, \zeta_2, 0) = \zeta_1 \zeta_2 \bar{\chi}^k(\xi), \qquad \zeta_1 + \zeta_2 = 1.$$

The latter condition follows from (4.2.8) with $\zeta_3 = 0$. Along Edge 4, ζ_1 ranges from 1 to 0 and ζ_2 ranges from 0 to 1 as ξ ranges from -1 to 1; thus, we may select

$$\zeta_1 = (1-\xi)/2, \qquad \zeta_2 = (1+\xi)/2, \qquad \zeta_3 = 0. \tag{4.4.6b}$$

While ξ may be defined in other ways, this linear mapping ensures that $\zeta_1 + \zeta_2 = 1$ on Edge 4. Compatibility with the edge shape function (4.4.2) requires

$$N_4^k(\zeta_1, \zeta_2, 0) = \bar{N}^k(\xi) = \frac{(1-\xi)(1+\xi)}{4}\bar{\chi}^k(\xi)$$

where $\bar{N}^k(\xi)$ is the one-dimensional hierarchical shape function (4.4.2e). Thus,

$$\bar{\chi}^k(\xi) = \frac{4\bar{N}^k(\xi)}{1-\xi^2}. \tag{4.4.6c}$$

The result can be written in terms of triangular coordinates by using (4.4.6b) to obtain $\xi = \zeta_2 - \zeta_1$; hence,

$$N_4^k(\zeta_1, \zeta_2, \zeta_3) = \zeta_1\zeta_2\bar{\chi}^k(\zeta_2 - \zeta_1), \qquad k = 2, 3, \ldots, p. \tag{4.4.7a}$$

Shape functions along other edges follow by permuting indices, *i.e.*,

$$N_5^k(\zeta_1, \zeta_2, \zeta_3) = \zeta_2\zeta_3\bar{\chi}^k(\zeta_3 - \zeta_2), \tag{4.4.7b}$$

$$N_6^k(\zeta_1, \zeta_2, \zeta_3) = \zeta_3\zeta_1\bar{\chi}^k(\zeta_1 - \zeta_3), \qquad k = 2, 3, \ldots, p. \tag{4.4.7c}$$

It might appear that the shape functions $\bar{\chi}^k(\xi)$ has singularities at $\xi = \pm 1$; however, the one-dimensional hierarchical shape functions have $(1-\xi^2)$ as a factor. Thus, $\bar{\chi}^k(\xi)$ is a polynomial of degree $k-2$. Using (2.5.8), the first four of them are

$$\bar{\chi}^2(\xi) = -\sqrt{6}, \qquad \bar{\chi}^3(\xi) = -\sqrt{10}\xi,$$
$$\bar{\chi}^4(\xi) = -\sqrt{\frac{7}{8}}(5\xi^2 - 1), \qquad \bar{\chi}^5(\xi) = -\sqrt{\frac{9}{8}}(7\xi^3 - 3\xi). \tag{4.4.8}$$

Interior shape functions. The $(p-1)(p-2)/2$ internal shape functions for $p \geq 3$ are products of the bubble function

$$N_7^{3,0,0} = \zeta_1\zeta_2\zeta_3 \tag{4.4.9a}$$

and Legendre polynomials. The Legendre polynomials are functions of two of the three triangular coordinates. Following Szabó and Babuška [7], we present them in terms of $\zeta_2 - \zeta_1$ and ζ_3. Thus,

$$N_7^{4,1,0} = N_7^{3,0,0}P_1(\zeta_2 - \zeta_1), \tag{4.4.9b}$$

$$N_7^{4,0,1} = N_7^{3,0,0}P_1(2\zeta_3 - 1), \tag{4.4.9c}$$

$$N_7^{5,2,0} = N_7^{3,0,0}P_2(\zeta_2 - \zeta_1), \tag{4.4.9d}$$

$$N_7^{5,1,1} = N_7^{3,0,0}P_1(\zeta_2 - \zeta_1)P_1(2\zeta_3 - 1), \tag{4.4.9e}$$

$$N_7^{5,0,2} = N_7^{3,0,0}P_2(2\zeta_3 - 1), \qquad \ldots. \tag{4.4.9f}$$

The shift in ζ_3 ensures that the range of the Legendre polynomials is $[-1, 1]$.

Like the edge shape functions for a square (4.4.2), the edge shape functions for a triangle (4.4.7) are products of a function on the edge ($\bar{\chi}^k(\zeta_i - \zeta_j)$) and a function ($\zeta_i\zeta_j$, $i \neq j$) that blends the edge function onto the element. However, the edge functions for the triangle are not the same as those for the square. The two are related by (4.4.6c). Having the same edge functions for all element shapes simplifies construction of the element stiffness matrices [6]. We can, of course, make the edge functions the same by redefining the blending functions. Thus, using (4.4.6a,c), the edge function for Edge 4 can be $\bar{N}^k(\xi)$ if the blending function is

$$\frac{4\zeta_1\zeta_2}{1-\xi^2}.$$

In a similar manner, using (4.4.2a) and (4.4.6c), the edge function for the shape function $N^k_{3,1}$ can be $\bar{\chi}^k(\xi)$ if the blending function is

$$\frac{\bar{N}_1(\eta)(1-\xi^2)}{4}.$$

Shephard *et al.* [6] show that representations in terms of $\bar{\chi}^k$ involve fewer algebraic operations and, hence, are preferred.

The first three edge and interior shape functions are shown in Figure 4.4.4. A degree p hierarchical approximation on a triangle has $3+3(p-1)_+ + (p-1)_+(p-2)_+/2$ unknowns and shape functions. This function is listed in Table 4.4.1. We see that for $p > 1$, there are two fewer shape functions with triangular elements than with squares. The triangular element is optimal in the sense of using the minimal number of shape functions for a complete polynomial of a given degree. This, however, does not mean that the complexity of solving a given problem is less with triangular elements than with quadrilaterals. This issue depends on the partial differential equations, the geometry, the mesh structure, and other factors.

Carnevali *et al.* [4] introduced shape functions that produce better conditioned element stiffness matrices at higher values of p than the bases presented here [7]. Adjerid *et al.* [1] construct an alternate basis that appears to further reduce ill conditioning at high p.

4.5 Three-Dimensional Shape Functions

Three-dimensional finite element shape functions are constructed in the same manner as in two dimensions. Common element shapes are tetrahedra and hexahedra and we will examine some Lagrange and hierarchical approximations on these elements.

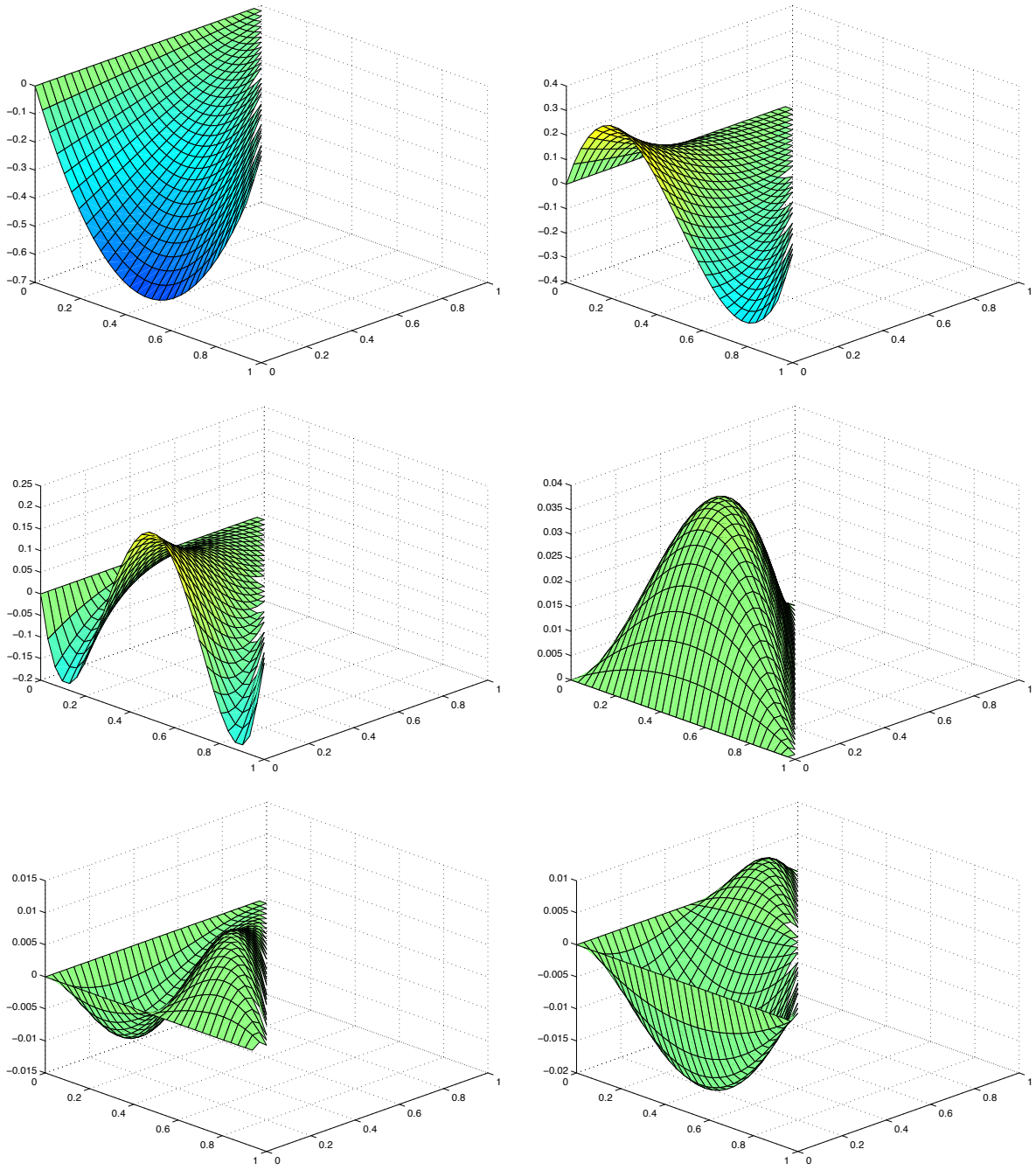

Figure 4.4.4: Hierarchical edge and interior shape functions N_4^2 (top left), N_4^3 (top right), N_4^4 (middle left), $N_7^{3,0,0}$ (middle right), $N_7^{4,1,0}$ (bottom left), $N_7^{4,0,1}$ (bottom right).

4.5.1 Lagrangian Shape Functions on Tetrahedra

Let us begin with a linear shape function on a tetrahedron. We introduce four nodes numbered (for convenience) as 1 to 4 at the vertices of the element (Figure 4.5.1). Imposing the usual Lagrangian conditions that $N_j(x_k, y_k, z_k) = \delta_{jk},\ j, k = 1, 2, 3, 4$, gives

the shape functions as

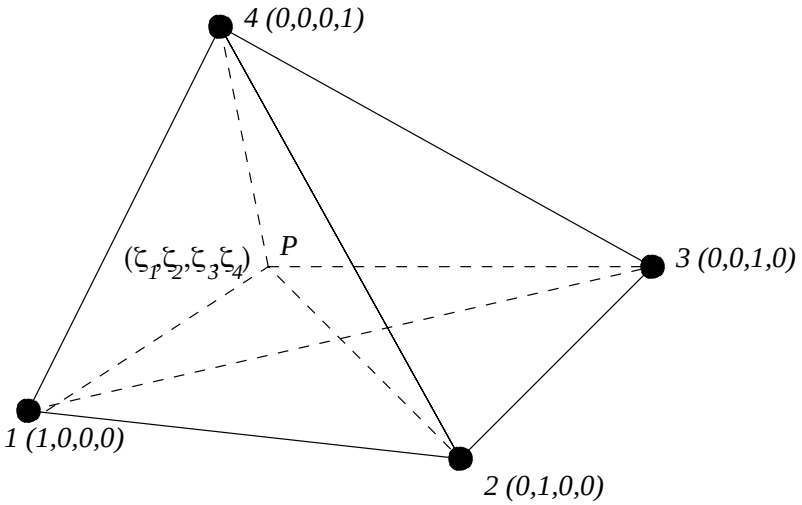

Figure 4.5.1: Node placement for linear shape functions on a tetrahedron and definition of tetrahedral coordinates.

$$N_j(x,y,z) = \frac{D_{k,l,m}(x,y,z)}{C_{j,k,l,m}}, \qquad (j,k,l,m) \text{ a permutation of } 1,2,3,4, \tag{4.5.1a}$$

where

$$D_{k,l,m}(x,y,z) = \det \begin{bmatrix} 1 & x & y & z \\ 1 & x_k & y_k & z_k \\ 1 & x_l & y_l & z_l \\ 1 & x_m & y_m & z_m \end{bmatrix}, \tag{4.5.1b}$$

$$C_{j,k,l,m} = \det \begin{bmatrix} 1 & x_j & y_j & z_j \\ 1 & x_k & y_k & z_k \\ 1 & x_l & y_l & z_l \\ 1 & x_m & y_m & z_m \end{bmatrix}. \tag{4.5.1c}$$

Placing nodes at the vertices produces a linear shape function on each face that is uniquely determined by its values at the three vertices on the face. This guarantees continuity of bases constructed from the shape functions. The restriction of U to element e is

$$U(x,y,z) = \sum_{j=1}^{4} c_j N_j(x,y,z). \tag{4.5.2}$$

As in two dimensions, we may construct higher-order polynomial interpolants by either mapping to a canonical element or by introducing "tetrahedral coordinates." Focusing on the latter approach, let

$$\zeta_j = N_j(x,y,z), \qquad j = 1,2,3,4, \tag{4.5.3a}$$

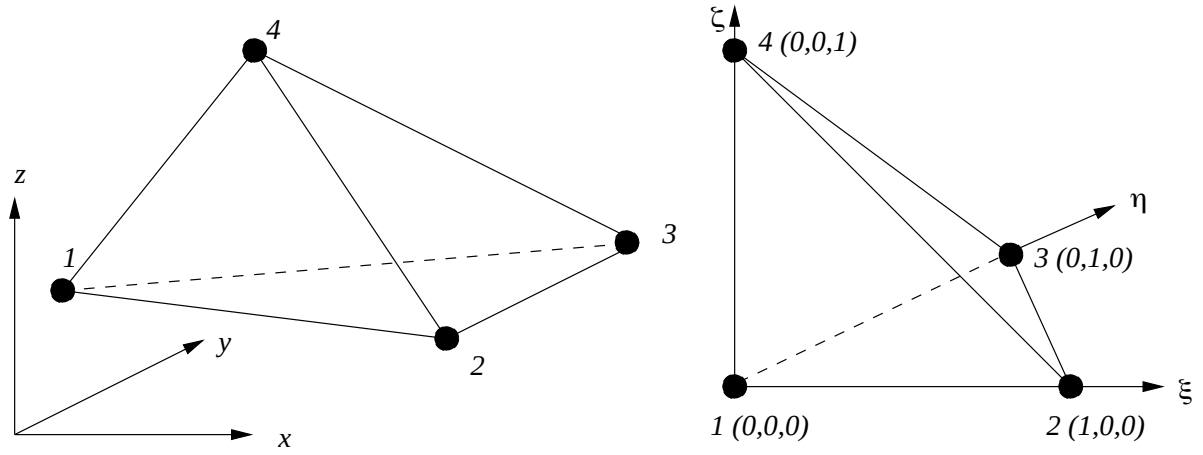

Figure 4.5.2: Transformation of an arbitrary tetrahedron to a right, unit canonical tetrahedron.

and regard ζ_j, $j = 1, 2, 3, 4$, as forming a redundant coordinate system on a tetrahedron. The coordinates of a point P located at $(\zeta_1, \zeta_2, \zeta_3, \zeta_4)$ are (Figure 4.5.1)

$$\zeta_1 = \frac{V_{P234}}{V_{1234}}, \qquad \zeta_2 = \frac{V_{P134}}{V_{1234}}, \qquad \zeta_3 = \frac{V_{P124}}{V_{1234}}, \qquad \zeta_4 = \frac{V_{P123}}{V_{1234}}, \tag{4.5.3b}$$

where V_{ijkl} is the volume of the tetrahedron with vertices at i, j, k, and l. Hence, the coordinates of Vertex 1 are $(1, 0, 0, 0)$, those of Vertex 2 are $(0, 1, 0, 0)$, *etc.* The plane $\zeta = 0$ is the plane A_{234} opposite to vertex 1, *etc.* The transformation from physical to tetrahedral coordinates is

$$\begin{bmatrix} x \\ y \\ z \\ 1 \end{bmatrix} = \begin{bmatrix} x_1 & x_2 & x_3 & x_4 \\ y_1 & y_2 & y_3 & y_4 \\ z_1 & z_2 & z_3 & z_4 \\ 1 & 1 & 1 & 1 \end{bmatrix} \begin{bmatrix} \zeta_1 \\ \zeta_2 \\ \zeta_3 \\ \zeta_4 \end{bmatrix}. \tag{4.5.4}$$

The coordinate system is redundant as expressed by the last equation.

The transformation of an arbitrary tetrahedron to a right, unit canonical tetrahedron (Figure 4.5.2) follows the same lines, and we may define it as

$$\xi = N_2(x, y, z), \qquad \eta = N_3(x, y, z), \qquad \zeta = N_4(x, y, z). \tag{4.5.5}$$

The face A_{134} (Figure 4.5.2) is mapped to the plane $\xi = 0$, the face A_{124} is mapped to $\eta = 0$, and A_{123} is mapped to $\zeta = 0$. In analogy with the two-dimensional situation, this transformation is really the same as the mapping (4.5.3) to tetrahedral coordinates.

A complete polynomial of degree p in three dimensions has

$$n_p = \frac{(p+1)(p+2)(p+3)}{6} \tag{4.5.6}$$

monomial terms (*cf.*, *e.g.*, Brenner and Scott [3], Section 3.6). With $p = 2$, we have $n_2 = 10$ monomial terms and we can determine Lagrangian shape functions by placing nodes at the four vertices and at the midpoints of the six edges (Figure 4.5.3). With $p = 3$, we have $n_3 = 20$ and we can specify shape functions by placing a node at each of the four vertices, two nodes on each of the six edges, and one node on each of the four faces (Figure 4.5.3). Higher degree polynomials also have nodes in the element's interior. In general there is 1 node at each vertex, $p-1$ nodes on each edge, $(p-1)(p-2)/2$ nodes on each face, and $(p-1)(p-2)(p-3)/6$ nodes in the interior.

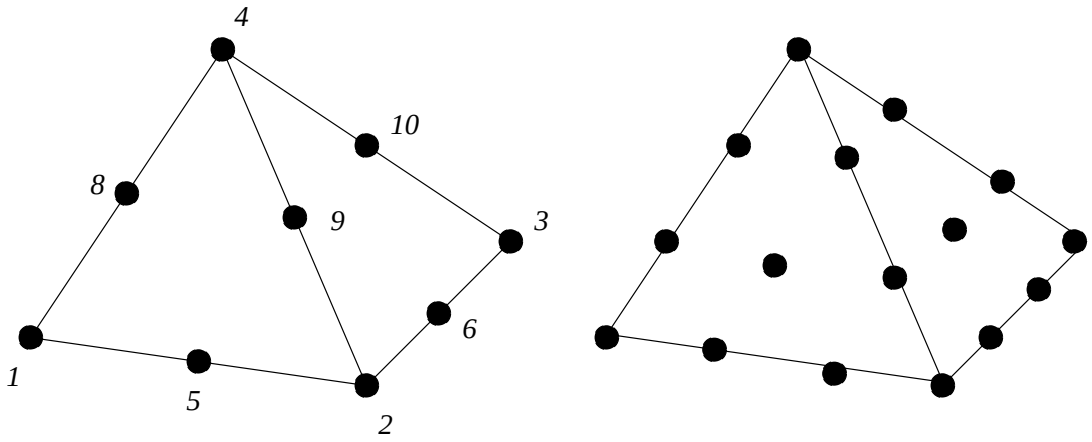

Figure 4.5.3: Node placement for quadratic (left) and cubic (right) interpolants on tetrahedra.

Example 4.5.1. The quadratic shape function N_1^2 associated with vertex Node 1 of a tetrahedron (Figure 4.5.3, left) is required to vanish at all nodes but Node 1. The plane $\zeta_1 = 0$ passes through face A_{234} and, hence, Nodes 2, 3, 4, 6, 9, 10. Likewise, the plane $\zeta_1 = 1/2$ passes through Nodes 5, 7 (not shown), and 8. Thus, N_1^2 must have the form

$$N_1^2(\zeta_1, \zeta_2, \zeta_3, \zeta_4) = \alpha\zeta_1(\zeta_1 - 1/2).$$

Since $N_1^2 = 1$ at Node 1 ($\zeta_1 = 1$), we find $\alpha = 2$ and

$$N_1^2(\zeta_1, \zeta_2, \zeta_3, \zeta_4) = 2\zeta_1(\zeta_1 - 1/2).$$

Similarly, the shape function N_5^2 associated with edge Node 5 (Figure 4.5.3, left) is required to vanish on the planes $\zeta_1 = 0$ (Nodes 2, 3, 4, 6, 9, 10) and $\zeta_2 = 0$ (Nodes 1, 3, 4, 7, 8, 10) and have unit value at Node 5 ($\zeta_1 = \zeta_2 = 1/2$). Thus, it must be

$$N_5^2(\zeta_1, \zeta_2, \zeta_3, \zeta_4) = 4\zeta_1\zeta_2.$$

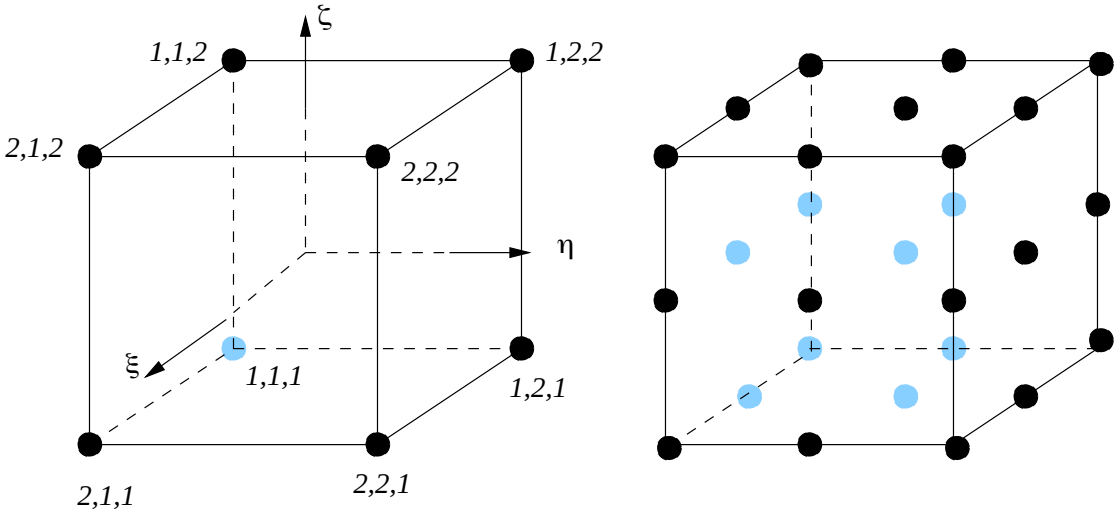

Figure 4.5.4: Node placement for a trilinear (left) and tri-quadratic (right) polynomial interpolants on a cube.

4.5.2 Lagrangian Shape Functions on Cubes

In order to construct a trilinear approximation on the canonical cube $\{\xi, \eta, \zeta | -1 \leq \xi, \eta, \zeta \leq 1\}$, we place eight nodes numbered (i, j, k), $i, j, k = 1, 2$, at its vertices (Figure 4.5.4). The shape function associated with Node (i, j, k) is taken as

$$N_{i,j,k}(\xi, \eta, \zeta) = \bar{N}_i(\xi)\bar{N}_j(\eta)\bar{N}_k(\zeta) \tag{4.5.7a}$$

where $\bar{N}_i(\xi)$, $i = 1, 2$, are the hat function (4.3.1d,e). The restriction of U to this element has the form

$$U(\xi, \eta, \zeta) = \sum_{i=1}^{2}\sum_{j=1}^{2}\sum_{k=1}^{2} c_{i,j,k} N_{i,j,k}(\xi, \eta, \zeta), \tag{4.5.7b}$$

Once again, $c_{i,j,k} = U_{i,j,k} = U(\xi_i, \eta_j, \zeta_k)$.

The placement of nodes at the vertices produces bilinear shape functions on each face of the cube that are uniquely determined by values at their four vertices on that face. Once again, this ensures that shape functions and U are C^0 functions on a uniform grid of cubes or rectangular parallelepipeds. Since each shape function is the product of one-dimensional linear polynomials, the interpolant is a trilinear function of the form

$$U(\xi, \eta, \zeta) = a_1 + a_2\xi + a_3\eta + a_4\zeta + a_5\xi\eta + a_6\eta\zeta + a_7\zeta\xi + a_8\xi\eta\zeta.$$

Other approximations and transformations follow their two-dimensional counterparts. For example, tri-quadratic shape functions on the canonical cube are constructed by placing 27 nodes at the vertices, midsides, midfaces, and centroid of the element (Figure 4.5.4). The shape function associated with Node (i, j, k) is given by (4.5.7a) with $\bar{N}_i(\xi)$ given by (4.3.3b-d).

4.5.3 Hierarchical Approximations

As with the two-dimensional hierarchical approximations described in Section 4.4, we use Szabó and Babuška's [7] shape function with the representation of Shephard *et al.* [6]. The basis for a tetrahedral or a canonical cube begins with the vertex functions (4.5.1) or (4.5.7), respectively. As noted in Section 4.4, higher-order shape functions are written as products

$$N_i^k(x,y,z) = \bar{\chi}^k(\xi,\eta,\zeta)\beta_i(\xi,\eta,\zeta) \tag{4.5.8}$$

of an entity function $\bar{\chi}^k$ and a blending function β_i.

- The *entity function* is defined on a mesh entity (vertex, edge, face, or element) and varies with the degree k of the approximation. It does not depend on the shapes of higher-dimensional entities.
- The *blending function* distributes the entity function over higher-dimensional entities. It depends on the shapes of the higher-dimensional entities but not on k.

The entity functions that are used to construct shape functions for cubic and tetrahedral elements follow.

Edge functions for both cubes and tetrahedra are given by (4.4.6c) and (4.4.2e) as

$$\bar{\chi}^k(\xi) = \frac{\sqrt{2(2k-1)}}{1-\xi^2}\int_{-1}^{\xi} P_{k-1}(\sigma)d\sigma, \qquad k \geq 2, \tag{4.5.9a}$$

where $\xi \in [-1,1]$ is a coordinate on the edge. The first four edge functions are presented in (4.4.8).

Face functions for squares are given by (4.4.3) divided by the square face blending function (4.4.3a)

$$\bar{\chi}^{k,\lambda,\mu}(\xi,\eta) = P_\lambda(\xi)P_\mu(\eta), \qquad \lambda+\mu = k-4, \qquad k \geq 4. \tag{4.5.9b}$$

Here, (ξ,η) are canonical coordinates on the face. The first six square face functions are

$$\begin{aligned} \bar{\chi}^{4,0,0} &= 1, & \bar{\chi}^{5,1,0} &= \xi, \\ \bar{\chi}^{5,0,1} &= \eta, & \bar{\chi}^{6,2,0} &= \frac{3\xi^2-1}{2}, \\ \bar{\chi}^{6,1,1} &= \xi\eta, & \bar{\chi}^{6,0,2} &= \frac{3\eta^2-1}{2}. \end{aligned}$$

Face functions for triangles are given by (4.4.9) divided the triangular face blending function (4.4.9a)

$$\bar{\chi}^{k,\lambda,\mu}(\zeta_1,\zeta_2,\zeta_3) = P_\lambda(\zeta_2-\zeta_1)P_\mu(2\zeta_3-1), \qquad \lambda+\mu = k-3, \qquad k \geq 3. \tag{4.5.9c}$$

As with square faces, $(\zeta_1, \zeta_2, \zeta_3)$ form a canonical coordinate system on the face. The first six triangular face functions are

$$\bar{\chi}^{3,0,0} = 1, \qquad \bar{\chi}^{4,1,0} = \zeta_2 - \zeta_1,$$
$$\bar{\chi}^{4,0,1} = 2\zeta_3 - 1, \qquad \bar{\chi}^{5,2,0} = \frac{3(\zeta_2 - \zeta_1)^2 - 1}{2},$$
$$\bar{\chi}^{5,1,1} = (\zeta_2 - \zeta_1)(2\zeta_3 - 1), \qquad \bar{\chi}^{5,0,2} = \frac{3(2\zeta_3 - 1)^2 - 1}{2}.$$

Now, let's turn to the blending functions.

The *tetrahedral element blending function* for an edge is

$$\beta_{ij}(\zeta_1, \zeta_2, \zeta_3, \zeta_4) = \zeta_i \zeta_j \tag{4.5.10a}$$

when the edge is directed from Vertex i to Vertex j. Using either Figure 4.5.2 or Figure 4.5.3 as references, we see that the blending function ensures that the shape function vanishes on the two faces not containing the edge to maintain continuity. Thus, if $i = 1$ and $j = 2$, the blending function for Edge $(1, 2)$ (which is marked with a 5 on the left of Figure 4.5.3) vanishes on the faces $\zeta_1 = 0$ (Face A_{234}) and $\zeta_2 = 0$ (Face A_{134}).

The blending function for a face is

$$\beta_{ijk}(\zeta_1, \zeta_2, \zeta_3, \zeta_4) = \zeta_i \zeta_j \zeta_k \tag{4.5.10b}$$

when the vertices on the face are i, j, and k. Again, the blending function ensures that the shape function vanishes on all faces but A_{ijk}. Again referring to Figures 4.5.2 or 4.5.3, the blending function β_{123} vanishes when $\zeta_1 = 0$ (Face A_{234}), $\zeta_2 = 0$ (Face A_{134}), and $\zeta_3 = 0$ (Face A_{124}).

The *cubic element blending function* for an edge is more difficult to write with our notation. Instead of writing the general result, let's consider an edge parallel to the ξ axis. Then

$$\beta_{1-2,j,k}(\xi, \eta, \zeta) = \frac{1 - \xi^2}{4} \bar{N}_j(\eta) \bar{N}_k(\zeta). \tag{4.5.11a}$$

The factor $(1 - \xi^2)/4$ adjusts the edge function to (4.5.9) as described in the paragraph following (4.4.9). The one-dimensional shape functions $\bar{N}_j(\eta)$ and $\bar{N}_k(\zeta)$ ensure that the shape function vanishes on all faces not containing the edge. Blending functions for other edges are obtained by cyclic permutation of ξ, η, and ζ and the index. Thus, referring to Figure 4.5.4, the edge function for the edge connecting vertices $2, 1, 1$ and $2, 2, 1$ is

$$\beta_{2,1-2,1}(\xi, \eta, \zeta) = \frac{1 - \eta^2}{4} \bar{N}_2(\xi) \bar{N}_1(\zeta).$$

Since $\bar{N}_2(-1) = 0$ (*cf.* (4.5.7b)), the shape function vanishes on the rear face of the cube shown in Figure 4.5.4. Since $\bar{N}_1(1) = 0$, the shape function vanishes on the top face of

the cube of Figure 4.5.4. Finally, the shape function vanishes at $\eta = \pm 1$ and, hence, on the left and right faces of the cube of Figure 4.5.4. Thus, the blending function (4.5.11a) has ensured that the shape function vanishes on all but the bottom and front faces of the cube of Figure 4.5.4.

The cubic face blending function for a face perpendicular to the ξ axis is

$$\beta_{i,j,k}(\xi,\eta,\zeta) = \bar{N}_i(\xi)(1-\eta^2)(1-\zeta^2). \tag{4.5.11b}$$

Referring to Figure 4.5.4, the quadratic terms in η and ζ ensure that the shape function vanishes on the right, left ($\eta = \pm 1$), top, and bottom ($\zeta = \pm 1$) faces. The one-dimensional shape function $\bar{N}_i(\xi)$ vanishes on the rear ($\xi = -1$) face when $i = 1$ and on the front ($\xi = 1$) face when $i = 2$; thus, the shape function vanishes on all faces but the one to which it is associated.

Finally, there are *elemental* shape functions. For tetrahedra, there are $(p-1)(p-2)(p-3)/6$ elemental functions for $p \geq 4$ that are given by

$$\begin{aligned} N_0^{k,\lambda,\mu,\nu}(\zeta_1,\zeta_2,\zeta_3,\zeta_4) &= \zeta_1\zeta_2\zeta_3\zeta_4 P_\lambda(\zeta_2-\zeta_1)P_\mu(2\zeta_3-1)P_\nu(2\zeta_4-1), \\ &\quad \forall\ \lambda+\mu+\nu = k-4, \qquad k = 4,5,\ldots,p. \end{aligned} \tag{4.5.12a}$$

The subscript 0 is used to identify the element's centroid. The shape functions vanish on all element faces as indicated by the presence of the multiplier $\zeta_1\zeta_2\zeta_3\zeta_4$. We could also split this function into the product of an elemental function involving the Legendre polynomials and the blend involving the product of the tetrahedral coordinates. However, this is not necessary.

For $p \geq 6$ there are the following elemental shape functions for a cube

$$N_0^{k,\lambda,\mu,\nu}(\xi,\eta,\zeta) = (1-\xi^2)(1-\eta^2)(1-\zeta^2)P_\lambda(\xi)P_\mu(\eta)P_\nu(\zeta), \qquad \forall\ \lambda+\mu+\nu = k-6. \tag{4.5.12b}$$

Again, the shape function vanishes on all faces of the element to maintain continuity. Adding, we see that there are $(p-5)_+(p-4)_+(p-3)_+/6$ element modes for a polynomial of order p.

Shephard *et al.* [6] also construct blending functions for pyramids, wedges, and prisms. They display several shape functions and also present entity functions using the basis of Carnevali *et al.* [4].

Problems

1. Construct the shape functions associated with a vertex, an edge, and a face node for a cubic Lagrangian interpolant on the tetrahedron shown on the right of Figure 4.5.3. Express your answer in the tetrahedral coordinates (4.5.3).

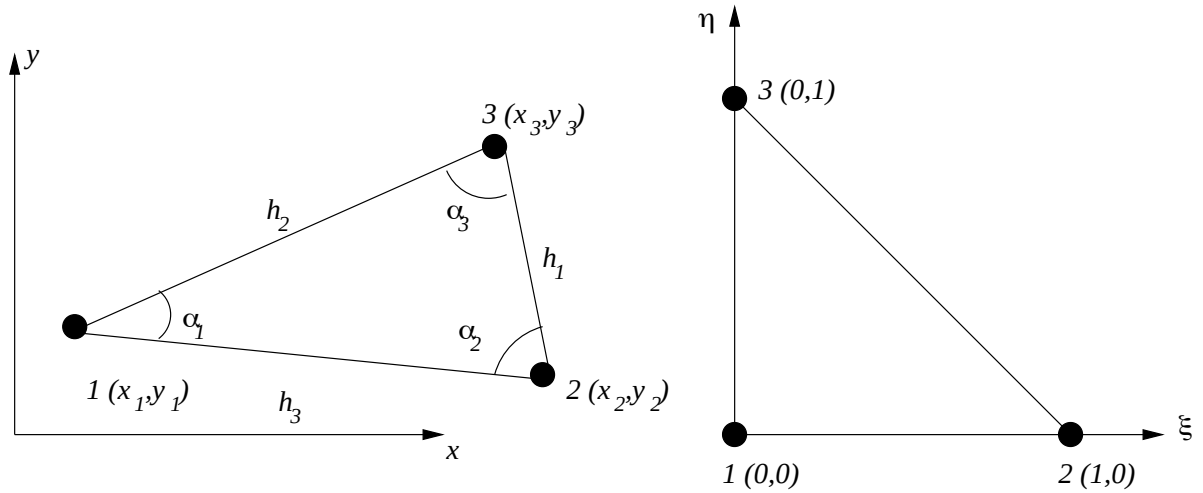

Figure 4.6.1: Nomenclature for a finite element in the physical (x, y)-plane and for its mapping to a canonical element in the computational (ξ, η)-plane.

4.6 Interpolation Error Analysis

We conclude this chapter with a brief discussion of the errors in interpolating a function u by a piecewise polynomial function U. This work extends our earlier study in Section 2.6 to multi-dimensional situations. Two- and three-dimensional interpolation is, naturally, more complex. In one dimension, it was sufficient to study limiting processes where mesh spacings tend to zero. In two and three dimensions, we must also ensure that element shapes cannot be too distorted. This usually means that elements cannot become too thin as the mesh is refined. We have been using coordinate mappings to construct bases. Concentrating on two-dimensional problems, the coordinate transformation from a canonical element in, say, the (ξ, η)-plane to an actual element in the (x, y)-plane must be such that no distorted elements are produced.

Let's focus on triangular elements and consider a linear mapping of a canonical unit, right, 45° triangle in the (ξ, η)-plane to an element e in the (x, y)-plane (Figure 4.6.1). More complex mappings will be discussed in Chapter 5. Using the transformation (4.2.8) to triangular coordinates in combination with the definitions (4.2.6) and (4.2.7) of the canonical variables, we have

$$\begin{bmatrix} x \\ y \\ 1 \end{bmatrix} = \begin{bmatrix} x_1 & x_2 & x_3 \\ y_1 & y_2 & y_3 \\ 1 & 1 & 1 \end{bmatrix} \begin{bmatrix} \zeta_1 \\ \zeta_2 \\ \zeta_3 \end{bmatrix} = \begin{bmatrix} x_1 & x_2 & x_3 \\ y_1 & y_2 & y_3 \\ 1 & 1 & 1 \end{bmatrix} \begin{bmatrix} 1-\xi-\eta \\ \xi \\ \eta \end{bmatrix}. \tag{4.6.1}$$

The Jacobian of this transformation is

$$\mathbf{J}_e := \begin{bmatrix} x_\xi & x_\eta \\ y_\xi & y_\eta \end{bmatrix}. \tag{4.6.2a}$$

Differentiating (4.6.1), we find the determinant of this Jacobian as

$$\det(\mathbf{J}_e) = (x_2 - x_1)(y_3 - y_1) - (x_3 - x_1)(y_2 - y_1). \tag{4.6.2b}$$

Lemma 4.6.1. *Let h_e be the longest edge and α_e be the smallest angle of Element e, then*

$$\frac{h_e^2}{2}\sin\alpha_e \le \det(\mathbf{J}_e) \le h_e^2 \sin\alpha_e. \tag{4.6.3}$$

Proof. Label the vertices of Element e as 1, 2, and 3; their angles as $\alpha_1 \le \alpha_2 \le \alpha_3$; and the lengths of the edges opposite these angles as h_1, h_2, and h_3 (Figure 4.6.1). With $\alpha_1 = \alpha_e$ being the smallest angle of Element e, write the determinant of the Jacobian as

$$\det(\mathbf{J}_e) = h_2 h_3 \sin\alpha_e.$$

Using the law of sines we have $h_1 \le h_2 \le h_3 = h_e$. Replacing h_2 by h_3 in the above expression yields the right-hand inequality of (4.6.3). The triangular inequality gives $h_3 < h_1 + h_2$. Thus, at least one edge, say, $h_2 > h_3/2$. This yields the left-hand inequality of (4.6.3). □

Theorem 4.6.1. *Let $\theta(x,y) \in H^s(\Omega_e)$ and $\tilde{\theta}(\xi,\eta) \in H^s(\Omega_0)$ be such that $\theta(x,y) = \tilde{\theta}(\xi,\eta)$ where Ω_e is the domain of element e and Ω_0 is the domain of the canonical element. Under the linear transformation (4.6.1), there exist constants c_s and C_s, independent of θ, $\tilde{\theta}$, h_e, and α_e such that*

$$c_s \sin^{s-1/2}\alpha_e h_e^{s-1}|\theta|_{s,\Omega_e} \le |\tilde{\theta}|_{s,\Omega_0} \le C_s \sin^{-1/2}\alpha_e h_e^{s-1}|\theta|_{s,\Omega_e} \tag{4.6.4a}$$

where the Sobolev seminorm is

$$|\theta|^2_{s,\Omega_e} = \sum_{|\boldsymbol{\kappa}|=s} \iint_{\Omega_e} (D^{\boldsymbol{\kappa}}\theta)^2 dxdy \tag{4.6.4b}$$

with $D^{\boldsymbol{\kappa}}u$ being a partial derivative of order $|\boldsymbol{\kappa}| = s$ (cf. Section 3.2).

Proof. Let us begin with $s = 0$, where

$$\iint_{\Omega_e} \theta^2 dxdy = \det(\mathbf{J}_e) \iint_{\Omega_0} \tilde{\theta}^2 d\xi d\eta$$

or

$$|\theta|^2_{0,\Omega_e} = \det(\mathbf{J}_e)|\tilde{\theta}|^2_{0,\Omega_0}.$$

Dividing by $\det(\mathbf{J}_e)$ and using (4.6.3)

$$\frac{|\theta|^2_{0,\Omega_e}}{\sin\alpha_e h_e^2} \le |\tilde{\theta}|^2_{0,\Omega_0} \le \frac{2|\theta|^2_{0,\Omega_e}}{\sin\alpha_e h_e^2}.$$

Taking a square root, we see that (4.6.4a) is satisfied with $c_0 = 1$ and $C_0 = \sqrt{2}$.

With $s = 1$, we use the chain rule to get

$$\theta_x = \tilde{\theta}_\xi \xi_x + \tilde{\theta}_\eta \eta_x, \qquad \theta_y = \tilde{\theta}_\xi \xi_y + \tilde{\theta}_\eta \eta_y.$$

Then,

$$|\theta|^2_{1,\Omega_e} = \iint_{\Omega_e} (\theta_x^2 + \theta_y^2) dx dy = \det(\mathbf{J}_e) \iint_{\Omega_0} (g_{1,e}\tilde{\theta}_\xi^2 + 2g_{2,e}\tilde{\theta}_\xi\tilde{\theta}_\eta + g_{3,e}\tilde{\theta}_\eta^2) d\xi d\eta$$

where

$$g_{1,e} = \xi_x^2 + \xi_y^2, \qquad g_{2,e} = \xi_x\eta_x + \xi_y\eta_y, \qquad g_{3,e} = \eta_x^2 + \eta_y^2.$$

Applying the inequality $ab \le (a^2 + b^2)/2$ to the center term on the right yields

$$|\theta|^2_{1,e} \le \det(\mathbf{J}_e) \iint_{\Omega_0} [g_{1,e}\tilde{\theta}_\xi^2 + g_{2,e}(\tilde{\theta}_\xi^2 + \tilde{\theta}_\eta^2) + g_{3,e}\tilde{\theta}_\eta^2] d\xi d\eta.$$

Letting

$$\delta = \max(|g_{1,e} + g_{2,e}|, |g_{3,e} + g_{2,e}|)$$

and using (4.6.4b), we have

$$|\theta|^2_{1,\Omega_e} \le \det(\mathbf{J}_e)\delta |\tilde{\theta}|^2_{1,\Omega_0}. \tag{4.6.5a}$$

Either by using the chain rule above with $\theta = x$ and y or by inverting the mapping (4.6.1), we may show that

$$\xi_x = \frac{y_\eta}{\det(\mathbf{J}_e)}, \qquad \xi_y = -\frac{x_\eta}{\det(\mathbf{J}_e)}, \qquad \eta_x = -\frac{y_\xi}{\det(\mathbf{J}_e)}, \qquad \eta_y = -\frac{x_\xi}{\det(\mathbf{J}_e)}.$$

From (4.6.2), $|x_\xi|$, $|x_\eta|$, $|y_\xi|$, $|y_\eta| \le h_e$; thus, using (4.6.3), we have $|\xi_x|$, $|\xi_y|$, $|\eta_x|$, $|\eta_y| \le 2/(h_e \sin\alpha_e)$. Hence,

$$\delta \le \frac{16}{(h_e \sin\alpha_e)^2}.$$

Using this result and (4.6.3) with (4.6.5a), we find

$$|\theta|^2_{1,\Omega_e} \le \frac{16}{\sin\alpha_e} |\tilde{\theta}|^2_{1,\Omega_0}. \tag{4.6.5b}$$

Hence, the left-hand inequality of (4.6.4a) is established with $c_1 = 1/4$.

To establish the right inequality, we invert the transformation and proceed from Ω_0 to Ω_e to obtain

$$|\tilde{\theta}|^2_{1,\Omega_0} \le \frac{\tilde{\delta}|\theta|^2_{1,\Omega_e}}{\det(\mathbf{J}_e)} \tag{4.6.6a}$$

with

$$\tilde{\delta} = \max(|\tilde{g}_{1,e} + \tilde{g}_{2,e}|, |\tilde{g}_{3,e} + \tilde{g}_{2,e}|),$$

$$\tilde{g}_{1,e} = x_\xi^2 + x_\eta^2, \qquad \tilde{g}_{2,e} = x_\xi y_\xi + x_\eta y_\eta, \qquad \tilde{g}_{3,e} = y_\xi^2 + y_\eta^2.$$

We've indicated that $|x_\xi|$, $|x_\eta|$, $|y_\xi|$, $|y_\eta| \le h_e$. Thus, $\tilde{\delta} \le 4h_e^2$ and, using (4.6.3), we find

$$|\tilde{\theta}|_{1,\Omega_0}^2 \le \frac{8}{\sin\alpha_e} |\theta|_{1,\Omega_e}^2. \tag{4.6.6b}$$

Thus, the right inequality of (4.6.4b) is established with $C_1 = 2\sqrt{2}$.

The remainder of the proof follows the same lines and is described in Axelsson and Barker [2]. □

With Theorem 4.6.1 established, we can concentrate on estimating interpolation errors on the canonical triangle. For simplicity, we'll use the Lagrange interpolating polynomial

$$\tilde{U}(\xi,\eta) = \sum_{j=1}^{n} \tilde{u}(\xi_j,\eta_j) N_j(\xi,\eta), \tag{4.6.7}$$

with n being the number of nodes on the standard triangle. However, with minor alterations, the results apply to other bases and, indeed, other element shapes. We proceed with one preliminary theorem and then present the main result.

Theorem 4.6.2. *Let p be the largest integer for which the interpolant (4.6.7) is exact when $\tilde{u}(\xi,\eta)$ is a polynomial of degree p. Then, there exists a constant $C > 0$ such that*

$$|\tilde{u} - \tilde{U}|_{s,\Omega_0} \le C|\tilde{u}|_{p+1,\Omega_0}, \qquad \forall u \in H^{p+1}(\Omega_0), \qquad s = 0, 1, \ldots, p+1. \tag{4.6.8}$$

Proof. The proof utilizes the Bramble-Hilbert Lemma and is presented in Axelsson and Barker [2]. □

Theorem 4.6.3. *Let Ω be a polygonal domain that has been discretized into a net of triangular elements Ω_e, $e = 1, 2, \ldots, N_\Delta$. Let h and α denote the largest element edge and smallest angle in the mesh, respectively. Let p be the largest integer for which (4.6.7) is exact when $\tilde{u}(\xi,\eta)$ is a complete polynomial of degree p. Then, there exists a constant $C > 0$, independent of $u \in H^{p+1}$ and the mesh, such that*

$$|u - U|_s \le \frac{C h^{p+1-s}}{[\sin\alpha]^s} |u|_{p+1}, \qquad \forall u \in H^{p+1}(\Omega), \qquad s = 0, 1. \tag{4.6.9}$$

Remark 1. The results are restricted $s = 0, 1$ because, typically, $U \in H^1 \cap H^{p+1}$.

Proof. Consider an element e and use the left inequality of (4.6.4a) with θ replaced by $u - U$ to obtain

$$|u - U|^2_{s,\Omega_e} \leq c_s^{-2} \sin^{-2s+1} \alpha_e h_e^{-2s+2} |\tilde{u} - \tilde{U}|^2_{s,\Omega_0}.$$

Next, use (4.6.8)

$$|u - U|^2_{s,\Omega_e} \leq c_s^{-2} \sin^{-2s+1} \alpha_e h_e^{-2s+2} C |\tilde{u}|^2_{p+1,\Omega_0}.$$

Finally, use the right inequality of (4.6.4a) to obtain

$$|u - U|^2_{s,\Omega_e} \leq c_s^{-2} \sin^{-2s+1} \alpha_e h_e^{-2s+2} C C^2_{p+1} \sin^{-1} \alpha_e h_e^{2p} |u|^2_{p+1,\Omega_e}.$$

Combining the constants

$$|u - U|^2_{s,\Omega_e} \leq C \sin^{-2s} \alpha_e h_e^{2(p+1-s)} |u|^2_{p+1,\Omega_e}.$$

Summing over the elements and taking a square root gives (4.6.9). □

A similar result for rectangles follows.

Theorem 4.6.4. *Let the rectangular domain Ω be discretized into a mesh of rectangular elements Ω_e, $e = 1, 2, \ldots, N_\Delta$. Let h and β denote the largest element edge and smallest edge ratio in the mesh, respectively. Let p be the largest integer for which (4.6.7) is exact when $\tilde{u}(\xi, \eta)$ is a complete polynomial of degree p. Then, there exists a constant $C > 0$, independent of $u \in H^{p+1}$ and the mesh, such that*

$$|u - U|_s \leq \frac{C h^{p+1-s}}{\beta^s} |u|_{p+1}, \qquad \forall u \in H^{p+1}(\Omega), \qquad s = 0, 1. \tag{4.6.10}$$

Proof. The proof follows the lines of Theorem 4.6.3 [2]. □

Thus, small and large (near π) angles in triangular meshes and small aspect ratios (the minimum to maximum edge ratio of an element) β in a rectangular mesh must be avoided. If these quantities remain bounded then the mesh is uniform as expressed by the following definition.

Definition 4.6.1. A family of finite element meshes Δ_h is *uniform* if all angles of all elements are bounded away from 0 and π and all aspect ratios are bounded away from zero as the element size $h \to 0$.

With such uniform meshes, we can combine Theorems 4.6.2, 4.6.3, and 4.6.4 to obtain a result that appears more widely in the literature.

Theorem 4.6.5. *Let a family of meshes Δ_h be uniform and let the polynomial interpolant U of $u \in H^{p+1}$ be exact whenever u is a complete polynomial of degree p. Then there exists a constant $C > 0$ such that*

$$|u - U|_s \leq C h^{p+1-s} |u|_{p+1}, \qquad s = 0, 1. \tag{4.6.11}$$

Proof. Use the bounds on α and β with (4.6.9) and (4.6.10) to redefine the constant C and obtain (4.6.11). □

Theorems 4.6.2 - 4.6.5 only apply when $u \in H^{p+1}$. If u has a singularity and belongs to H^{q+1}, $q < p$, then the convergence rate is reduced to

$$|u - U|_s \leq C h^{q+1-s} |u|_{q+1}, \qquad s = 0, 1. \tag{4.6.12}$$

Thus, there appears to be little benefit to using p *th*-degree piecewise-polynomial interpolants in this case. However, in some cases, highly graded nonuniform meshes can be created to restore a higher convergence rate.

Bibliography

[1] S. Adjerid, M. Aiffa, and J.E. Flaherty. Hierarchical finite element bases for triangular and tetrahedral elements. *Computer Methods in Applied Mechanics and Engineering*, 2000. to appear.

[2] O. Axelsson and V.A. Barker. *Finite Element Solution of Boundary Value Problems.* Academic Press, Orlando, 1984.

[3] S.C. Brenner and L.R. Scott. *The Mathematical Theory of Finite Element Methods.* Springer-Verlag, New York, 1994.

[4] P. Carnevali, R.V. Morric, Y.Tsuji, and B. Taylor. New basis functions and computational procedures for p-version finite element analysis. *International Journal of Numerical Methods in Enginneering*, 36:3759–3779, 1993.

[5] S. Dey, M.S. Shephard, and J.E. Flaherty. Geometry-based issues associated with p-version finite element computations. *Computer Methods in Applied Mechanics and Engineering*, 150:39 – 50, 1997.

[6] M.S. Shephard, S. Dey, and J.E. Flaherty. A straightforward structure to construct shape functions for variable p-order meshes. *Computer Methods in Applied Mechanics and Engineering*, 147:209–233, 1997.

[7] B. Szabó and I. Babuška. *Finite Element Analysis.* John Wiley and Sons, New York, 1991.

[8] O.C. Zienkiewicz. *The Finite Element Method.* McGraw-Hill, New York, third edition, 1977.